BNL-79261-2007-IR

Low-fidelity cross section covariances for 219 fission products in the fast neutron region

M.T. Pigni[1], M. Herman, P. Oblozinsky, D.Rochman

Energy Sciences & Technology Department
National Nuclear Data Center
Brookhaven National Laboratory
P.O. Box 5000
Upton, NY 11973-5000
www.bnl.gov

August 27, 2007

Keywords: Covariance, Uncertainty, Fission products

[1]Reference Author: pigni@bnl.gov

DISCLAIMER

Contents

Abstract

An extensive set of covariances for neutron cross sections in the energy range 5 keV-20 MeV has been developed to provide initial, low-fidelity but consistent uncertainty data for nuclear criticality safety applications. The methodology for the determination of such covariances combines the nuclear reaction model code EMPIRE, which calculates sensitivity to nuclear reaction model parameters, and the Bayesian code KALMAN to propagate uncertainty of the model parameters to cross sections. Taking into account the large scale of the project (219 fission products), only partial reference to experimental data has been made. Therefore, the covariances are, to a large extent, derived from the perturbation of several critical model parameters selected through the sensitivity analysis. These parameters define optical potential, level densities and pre-equilibrium emission. This work represents the first attempt ever to generate nuclear data covariances on such a scale.

Chapter 1

Introduction

Neutron cross section covariance information is required for a number of applications. Probably the most active user group requiring these data is related to nuclear criticality safety. Computational tools used or being developed for this application need huge amount of covariance data, ideally for all materials included in the evaluated nuclear data libraries such as recently released ENDF/B-VII.0 [1]. This would guarantee that the calculated values of neutron multiplication factor, k_{eff}, and their uncertainties can be predicted for variety of criticality experiments using different composition of materials at different energies.

The other applications where neutron covariance data are in high demand include advanced nuclear reactor systems and fuel cycles. These applications are pursued by the U.S. Department of Energy and include Global Nuclear Energy Partnership GNEP, new generation of power reactors GEN-IV and Advanced Fuel Cycle Initiative AFCI. The problem is that the availability of covariances in the major nuclear data libraries is very limited. For example, the most recent ENDF/B-VII.0 library, released in December 2006, contains covariances for 26 materials only, i.e., for less than 7% of the materials included in the neutron sub-library. Only half of them covers all reaction channels important for applications and can be, therefore, considered complete. Lack of consistent and complete set of covariances is a barrier that prevents using the sensitivity tools in the development of innovative nuclear technologies and discourages advancement of the tools themselves.

In order to meet nuclear criticality safety requirements and allow for testing and further development of their computational tools, the "low-fidelity" covariance project for nuclear criticality safety has been initiated. Its goal is to produce rough set of covariances covering all relevant reaction chan-

nels and materials, from the thermal energy to 20 MeV. The emphasis is on the completeness rather than on the precision - the latter should come later once the evaluation methodology is well established and adequate tools made available.

The low-fidelity covariance project involves four national laboratories, BNL, LANL, ORNL and ANL. The role of BNL is to produce covariances in the fast neutron region (5 keV - 20 MeV) for 304 materials, ^{19}F - ^{209}Bi. This massive task was split into two parts, fission products (219 materials in the range Z = 31 - 68), to be followed by 57 structural materials and 28 heavy materials. The present report is devoted to our results for fission product materials, recently presented at the international conference [5], and fully reported here.

The report is organized as follows. In Chapter 2 we describe the methodology and in Chapter 3 our results. This is followed by our conclusions in Chapter 4.

Chapter 2

Scope and Methodology

The aim of the low-fidelity neutron cross section covariance project is to produce file MF33 (cross section covariances) for a complete set of materials included in the ENDF/B-VII.0 neutron sub-library. The data should cover 5 major reaction channels, (n,el), (n,inl), (n,2n), (n,γ) and (n,f), with the understanding that (n,tot) is redundant. The project involves four national laboratories with the following responsibilities:

- ORNL - Low neutron energy region (<5 keV) for all nuclei
- BNL - Fast neutron energy region (5 keV - 20 MeV) for nuclei 19≤A≤209
- LANL - Fast neutron energy region (5 keV - 20 MeV) for light nuclei A≤18 and for actinides A≥210
- ANL - Checking and reviewing

Apart from actinides and light nuclei, BNL should produce covariances for the remaining 304 materials in the new ENDF/B-VII.0 library (see Tab. 2.1).

Table 2.1: List of 304 materials to be evaluated by BNL. The list covers all materials in the neutron sub-library of ENDF/B-VII.0, from ^{19}F to ^{209}Bi.

Materials	Nuclei	No. of isotopes
Structural	^{19}F - ^{nat}Zn	57
Fission products	^{69}Ga - ^{170}Er	219
Heavy	^{175}Lu - ^{209}Bi	28

The methodology used in the present work is based on the BNL nuclear reaction model code EMPIRE [2] coupled to the LANL Bayesian filtering

code KALMAN [3]. In view of the large scale of the present project, the results are fully based on model calculations without reference to experimental data. The EMPIRE code allows model calculations using a proper choice of model of parameter values leading to a complete set of evaluated cross sections, while KALMAN propagates the model parameter uncertainties into cross section (co)variances. A first set of covariance data for fission product materials has been presented by M.T. Pigni at the recent international conference [5].

In Section 2.1, we present the general concept of the procedure to determine uncertainties and related covariance matrices. Section 2.2 gives an overview of model parameters to which calculated cross sections are most sensitive. Then, the results and the applicability of the method is demonstrated in Section 2.3.

2.1 Evaluation method

The EMPIRE-KALMAN method combines physics modeling of nuclear reactions with the Bayesian update procedure, which is a standard tool used in statistics to evaluate the effect of the new data. The evaluation starts with the EMPIRE nuclear reaction model code which makes use of a wide range of nuclear models of different degree of sophistication in order to provide an overall description of nuclear observables. The adopted models address specific reaction mechanisms and are characterized by adjustable parameters. The most relevant model parameters are those related to optical potential and nuclear level densities. These parameters are varied to calculate partial derivatives of cross sections and thus defining the elements of the sensitivity matrices (e.g. Eq. 2.3). Thus, calculated reaction cross sections, sensitivity matrices along with the model parameters and their uncertainties represent input quantities for the KALMAN code.

The code KALMAN is used as a nuclear data evaluation tool based on the iterative least-square approach. The procedure puts emphasis on the estimation of the model parameter uncertainties and the corresponding correlations. The procedure is then applied to the evaluation of neutron cross sections and their covariance matrices for various reaction channels. The application of the Bayesian equations is straightforward and the update is a simple algebraic operation,

$$\mathbf{x}^{(n+1)} = \mathbf{x}^{(n)} + \mathbf{X}^{(n)}\mathbf{A}^{\mathrm{T}}\mathbf{Q}^{(n)}(\boldsymbol{\eta}^{(n)} - \boldsymbol{\sigma}(\mathbf{x}^{(n)}))$$

$$\mathbf{X}^{(n+1)} = \mathbf{X}^{(n)} - \mathbf{X}^{(n)}\mathbf{A}^{\mathrm{T}}\mathbf{Q}^{(n)}\mathbf{A}\mathbf{X}^{(n)}\,, \tag{2.1}$$

where n denotes the n^{th}-step in the evaluation process according to the number of sets of experimental data to be included. The vector $\mathbf{x}^{(n+1)}$ contains the improved values of the parameters starting from the vector $\mathbf{x}^{(n)}$. Likewise, the matrix $\mathbf{X}^{(n+1)}$ is the updated covariance matrix of the parameters $\mathbf{x}^{(n+1)}$. The combination between experimental and theoretical covariance matrices results in the updated error matrix, $\mathbf{Q} = (\mathbf{W} + \mathbf{V})^{-1}$, where $\mathbf{V}$ is the covariance matrix corresponding to the experimental cross sections $\boldsymbol{\eta}$. The vector $\boldsymbol{\sigma}(\mathbf{x})$ represents the set of cross sections for a specific reaction channel (total, elastic, capture,...) calculated for the set of parameters $\mathbf{x}$. The corresponding covariance matrix,

$$\mathbf{W} = \mathbf{A}\mathbf{X}\mathbf{A}^{\mathrm{T}} \tag{2.2}$$

is associated with a model calculation by the correlation matrix of the model parameters, $\mathbf{X} \equiv \langle \Delta x_\ell \Delta x_m \rangle$, and the sensitivity matrix $\mathbf{A}$ with elements,

$$a_{i,j} = \frac{\partial \sigma(\mathbf{x}, E_i)}{\partial x_j}\,. \tag{2.3}$$

calculated at the energy E_i.

2.2 Models and their parameters

EMPIRE code system is a modern tool for modeling nuclear reactions, which is mainly used for data evaluations. The code incorporates an extended set of nuclear reaction models capable of simulating all relevant reaction mechanisms. Therefore, EMPIRE provides reasonable overall description of nuclear observables even if default parametrization is being used. The advantage of EMPIRE is the simplicity of the input, default values for all parameters and wide range of target mass number ($A \gtrsim 19$) and incident energies (0.1 keV $\lesssim E \lesssim 50$ MeV).

For the purposes of this project the following nuclear reactions models were adopted:

- Spherical optical model
- Hauser-Feshbach statistical model
- Exciton pre-equilibrium model

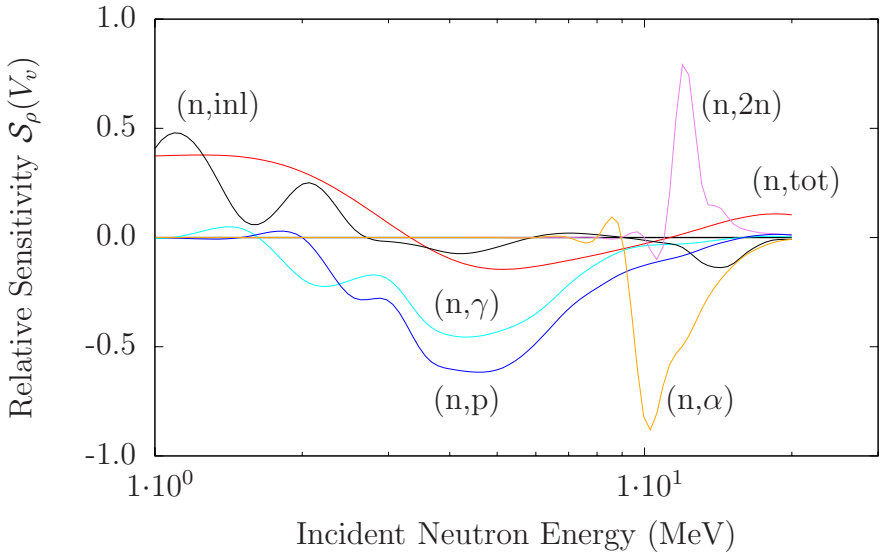

Figure 2.1: Energy dependence of the relative sensitivity to V_v for the most important neutron induced reactions on ^{89}Y. V_v has been varied by $\Delta V_v = \pm 5\%$ (see Eq. 2.4).

The input model parameters listed in Tabs. 2.2 and 2.3 are those that contribute most significantly to cross sections and their uncertainties. They include 10 parameters for optical model potential and 8 parameters for nuclear level densities as well as pre-equilibrium decay.

The effect of a perturbation of a model parameter on cross sections is determined via the relation

$$\mathcal{S}_\rho(E,k) = \frac{\sigma_\rho^{(+)}(E,k) - \sigma_\rho^{(-)}(E,k)}{\sigma_\rho^{(0)}(E)}\,, \tag{2.4}$$

where,

$$\sigma_\rho^{(0)}(E) = \sigma_\rho(E; x_1, \ldots, x_j)$$

is the value of the cross section calculated for the best (or default) set of parameters $\mathbf{x} = (x_1, \ldots, x_j)$ for a specific reaction channel ρ, while

$$\sigma_\rho^{(\pm)}(E,k) = \sigma_\rho^{(\pm)}(E; x_1, x_2, \ldots, x_k \pm \delta x_k, \ldots, x_j)$$

are cross sections calculated with the value of the parameter k perturbed by its expected uncertainty δx_k. We note that $S_\rho(E,k)$ is related to the

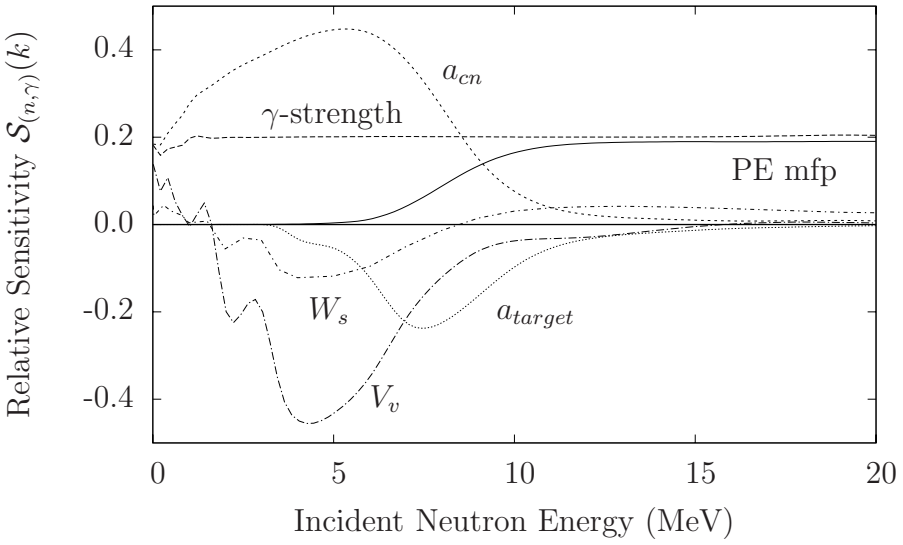

Figure 2.2: Relative sensitivity of the ^{89}Y(n,γ) reaction, to the perturbation of level density and optical model parameters by ±5% and γ-ray as well as pre-equilibrium strength by ±10%.

sensitivity matrix a through

$$\mathcal{S}_\rho(E,k) = 2a_{(E,k)}\delta x_k \tag{2.5}$$

and is a convenient measure of the cross section response to the physically sensible variation of the model parameter k.

Fig. 2.1 shows examples of such response to the variation of the real depth of the optical potential V_v. The reaction channels plotted in Fig. 2.1 display remarkably different levels of sensitivity and distinct energy dependence. Fig. 2.2 shows response of the neutron radiative capture on ^{89}Y to the variation of the dominating parameters. It is obvious that some model parameters generate small or negligible perturbations on all reaction channels, while others have an important effect only on a specific ones. Two fundamental nuclear reaction mechanisms are clearly evident. In the energy region below 10 MeV, the neutron capture is described by the formation and decay of the compound nucleus. As expected, the nuclear level density parameters a_{cn} and a_{tg} play an important role along with the depths of the real volume V_v and imaginary surface W_s components of optical model potential for neutrons. At higher energies the pre-equilibrium emission mechanism becomes dominant and the mean free path parameter (PE mfp) plays the major role. The radiative strength function enters as a multiplicative factor

Table 2.2: Percentage uncertainties used for the optical model parameters [4]. The subscripts v and s indicate real volume and surface components, while w refers the imaginary surface. The r and a are the radius and diffuseness parameters defining the Wood-Saxon potential, while V and W are the real and imaginary well depths, respectively. 'tg' superscripts indicate neutron plus target ($^{A}_{Z}$X) channel, while 'np' refers to a proton plus $^{A+1}_{Z-1}$X system.

	$\Delta r_s^{(tg)}$	$\Delta r_v^{(tg)}$	$\Delta r_w^{(tg)}$	$\Delta V_v^{(tg)}$	$\Delta W_s^{(tg)}$
%	± 3.0	± 3.0	± 3.0	± 3.0	± 5.0
	$\Delta W_v^{(tg)}$	$\Delta a_s^{(tg)}$	$\Delta a_v^{(tg)}$	$\Delta V_v^{(np)}$	$\Delta W_s^{(np)}$
%	± 5.0	± 3.0	± 3.0	± 3.0	± 3.0

in all mechanisms, therefore its role is practically constant.

The uncertainties of the model parameters used in the covariance calculations are given in Tabs. 2.2 and 2.3. They define the diagonal matrix **X**.

Table 2.3: Percentage uncertainties of nuclear level densities $\tilde{a}$ and single particle level densities $\tilde{g}$ (pre-equilibrium emission) parameters. The subscripts relate these quantities to the nuclei - $cn \equiv$ compound, $tg \equiv$ target, $n2n \equiv$ (n,2n) residue, $np \equiv$ (n,p) residue. The uncertainties on the γ-ray strength functions are applied to all nuclei and on those for the pre-equilibrium mean free path apply to the compound (composite) nucleus only.

	$\Delta\tilde{a}^{(cn)}$	$\Delta\tilde{a}^{(tg)}$	$\Delta\tilde{a}^{(n2n)}$	$\Delta\tilde{a}^{(np)}$
%	± 10	± 10	± 10	± 10
	$\Delta\tilde{g}^{(np)}$	$\Delta\tilde{g}^{(tg)}$	$\Delta(\gamma\text{-}strength)$	Δ(PE mfp)
%	± 10	± 10	± 20	± 20

2.3 Example

The cross section covariances were calculated for 219 isotopes at 30 incident energies between 5 keV and 20 MeV. The five reaction channels considered in the present example were total, elastic, inelastic, capture, and (n,2n). Altogether, 18 model parameters were varied in the calculations. The results

are fully based on model calculations and while experimental data were not taken into account, they were occasionally consulted to get a better feeling about the quality of produced results. This is in line with the intention of the project which aims to produce low-fidelity covariances for an extensive set of nuclei.

The cross section uncertainties were determined by the procedure presented in Section 2.1. The neutron cross sections were calculated using a default set of model parameters common to all considered nuclei. The covariance matrices were calculated by the KALMAN code and, in explicit notation, they are

$$w_{i,j} = \sum_{\ell,m=1}^{J} \frac{\partial\sigma(\mathbf{x};E_i)}{\partial x_\ell}\langle\Delta x_\ell \Delta x_m\rangle \frac{\partial\sigma(\mathbf{x};E_j)}{\partial x_m}\,, \tag{2.6}$$

where $\mathbf{X} \equiv \langle\Delta x_\ell \Delta x_m\rangle$ is the correlation matrix of the model parameters. The matrix $\mathbf{X}$ is diagonal, because we assumed that model parameters are uncorrelated, with uncertainties given in the Tab. 2.2. In general, the covariance matrices are normalized,

$$\zeta_{i,j} = \frac{w_{i,j}}{\sqrt{w_{i,i}}\sqrt{w_{j,j}}}\,, \tag{2.7}$$

which by definition leads to matrix elements in the range of $-1 \leq \zeta_{i,j} \leq 1$. We remind that covariance matrices must be symmetric and definite positive, namely

$$\mathbf{ZWZ}^{\mathrm{T}} > 0\,, \tag{2.8}$$

for all non-zero real vectors. Numerical rounding errors in the normalization procedure expressed by Eq. 2.7 can lead to inconsistencies and matrices, $\boldsymbol{\zeta}$, not satisfying the condition of Eq. 2.8. In Figs. 2.3-2.5 relative uncertainties for the most important reaction channels ^{127}I+n are shown as an example. The total and elastic channels obviously exhibit similar structure characterized by the presence of the nodes, where the uncertainties become considerably smaller. This is due to the low sensitivity of the cross sections to the optical potential parameters at these particular energies. One can also notice that uncertainties for these two reaction channels become relatively high at low energies and for ≈0.5 and ≈3 MeV. Inelastic and capture reveal expected high uncertainties for energies ≳15 MeV, while, essentially flat shape is obtained for (n,2n) except of the threshold region.

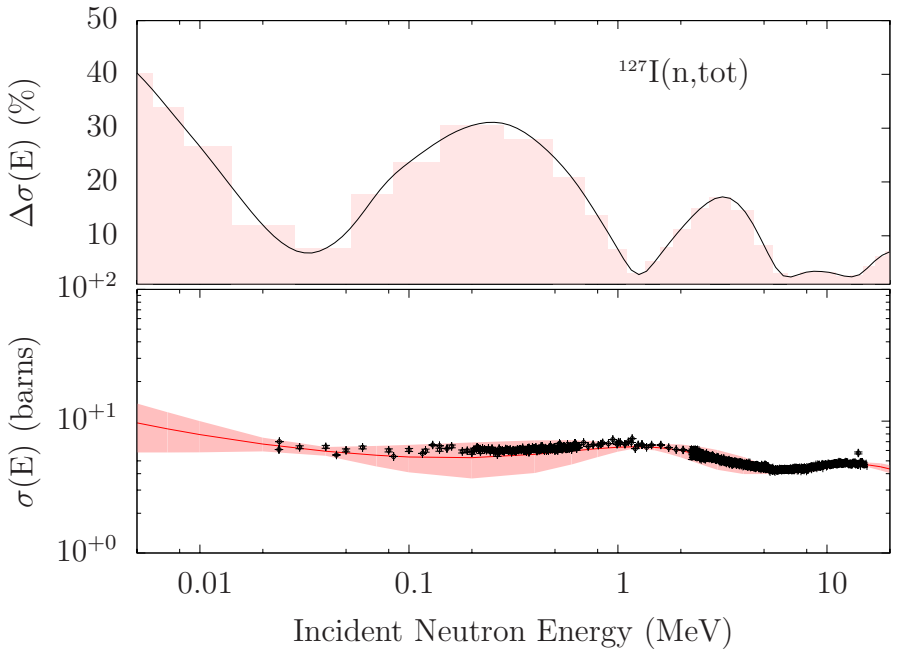

Figure 2.3: Relative uncertainties for ^{127}I(n,tot) and ^{127}I(n,el) obtained with the EMPIRE-KALMAN method and plotted along with the cross section and experimental data.

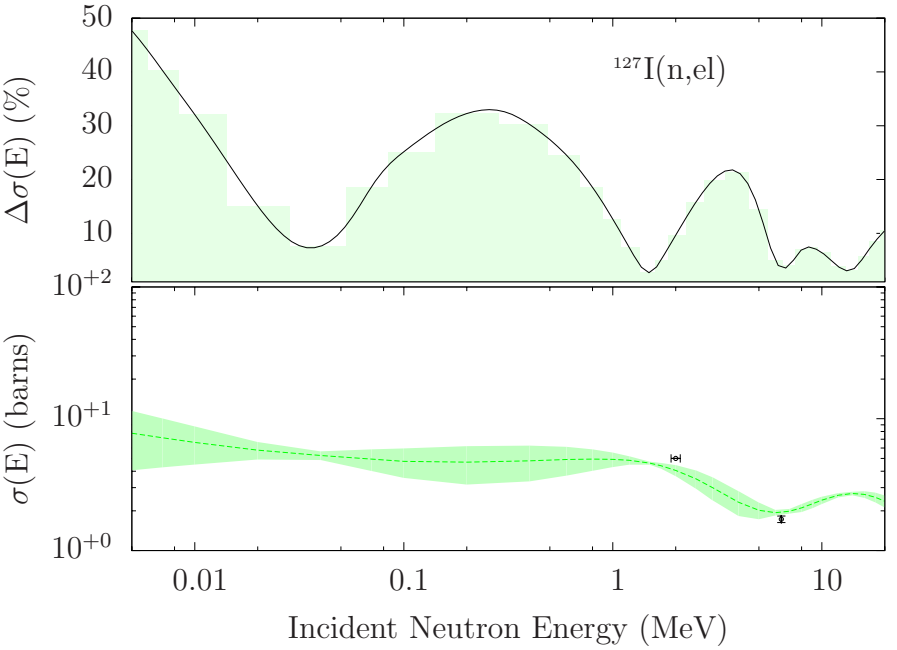

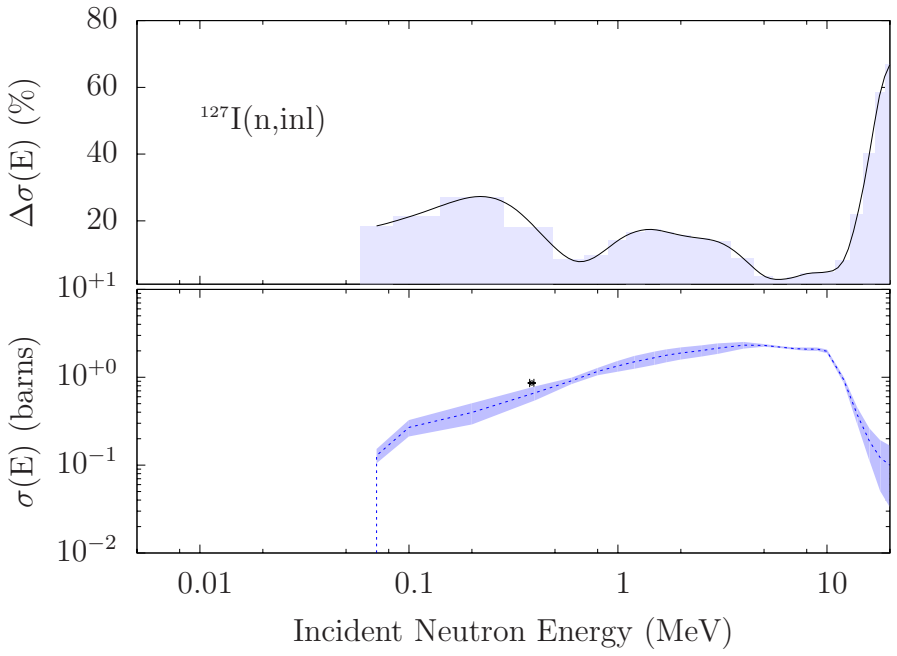

Figure 2.4: Relative uncertainties for ^{127}I(n,inl) and ^{127}I(n,2n) obtained with the EMPIRE-KALMAN method and plotted along with the cross section and experimental data.

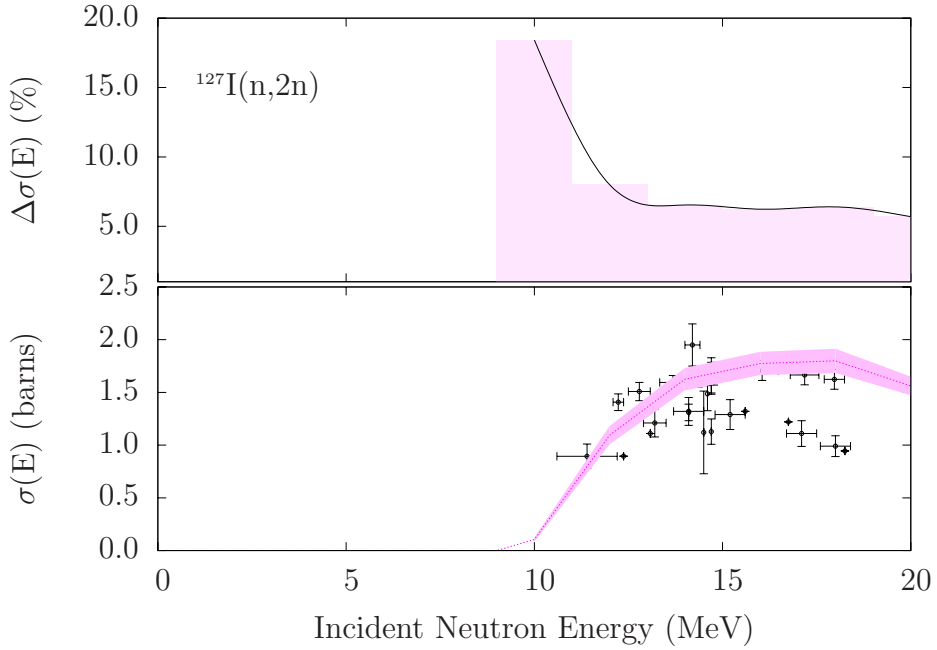

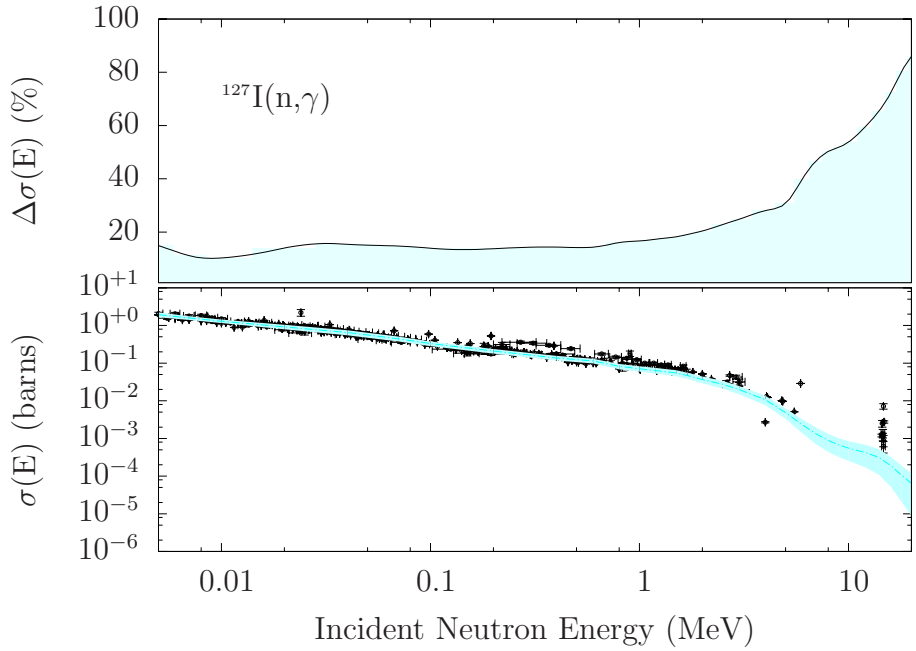

Figure 2.5: Relative uncertainties for ^{127}I(n,γ) obtained with the EMPIRE-KALMAN method and plotted along with the cross section and experimental data.

Chapter 3

Results

The obtained neutron cross section covariance matrices were calculated for 219 isotopes at 30 incident energies between 5 keV and 20 MeV (see Tab. 3.1). The four reaction channels considered in the present work were elastic, inelastic, capture, and (n,2n). Altogether, 18 model parameters were varied in the calculations. The results are totally based on model calculations and no experimental data were taken into account. The uncertainties were determined following the procedure presented in 2.1 and the list of 219 nuclei is given in Tabs. 3.3.

Table 3.1: List of 30 energies used in the calculations of cross section covariances.

No.	Energy (MeV)	No.	Energy (MeV)	No.	Energy (MeV)
1	0.005	11	0.800	21	6.000
2	0.007	12	1.000	22	7.000
3	0.010	13	1.200	23	8.000
4	0.020	14	1.500	24	9.000
5	0.040	15	1.700	25	10.00
6	0.070	16	2.000	26	12.00
7	0.100	17	2.500	27	14.00
8	0.200	18	3.000	28	16.00
9	0.400	19	4.000	29	18.00
10	0.600	20	5.000	30	20.00

Figs. 3.1-3.20 show relative uncertainties for the required reaction channels. These figures refer to 10 isotopes (see Tab. 3.2), out of 219 fission product materials, already sent to ORNL for testing and merging with their

low energy covariances (<5 keV) into a single file MF33.

As already discussed in Section 2.3, the elastic channel generally shows a structure characterized by the presence of nodes, where the uncertainties are sensibly small. These oscillations could be seen to result from the scattering resonances present in the structure of neutron cross sections. The essential feature, here, is the consideration of the interference of that part of the incident neutron wave which traverses the nucleus with the part of the wave which has gone around. The determination of the phase shifts plays a main role in predicting theoretically the origin of these oscillations. Furthermore, the widths and the positions of the maxima positions are likely related to the parameter of real potential well and the nuclear radius.

The same considerations can not be extended to the non-elastic reaction channels because level densities parameters play a main role in the cross section calculations. In general, inelastic and capture channels reveal expected high uncertainties for energies $\gtrsim$15 MeV, while, essentially flat shape is obtained for (n,2n) except of the threshold region and energies $\approx$20 MeV.

Table 3.2: List of 10 nuclei, out of 219 fission product materials, sent to ORNL in July 2007 for testing and merging with their low energy data.

No.	Materials	No.	Materials
1	^{83}Kr	6	^{131}Xe
2	^{91}Zr	7	^{134}Ba
3	^{103}Rh	8	^{145}Nd
4	^{109}Ag	9	^{149}Sm
5	^{113}Cd	10	^{152}Eu

In Figs. 3.21-3.25 percentage relative uncertainties for the major reaction channels are shown in a contour plot where the numbers on x and y axes refer to the complete list of fission product nuclei and the number of energy bins respectively. The exceptionally high uncertainties are found for nuclei between Xe and Eu below 100 keV. A possible explanation of this effect can be traced to the structure observed in the s- and/or d-wave neutron strength functions.

Table 3.3: List of fission product materials evaluated by BNL. The list corresponds to the neutron sub-library of the ENDF/B-VII.0 library [1].

No.	Material	MAT		No.	Material	MAT
1)	^{69}Ga	3125		38)	^{90}Zr	4025
2)	^{71}Ga	3131		39)	^{91}Zr	4028
3)	^{70}Ge	3225		40)	^{92}Zr	4031
4)	^{72}Ge	3231		41)	^{93}Zr	4034
5)	^{73}Ge	3234		42)	^{94}Zr	4037
6)	^{74}Ge	3237		43)	^{95}Zr	4040
7)	^{76}Ge	3243		44)	^{96}Zr	4043
8)	^{74}As	3322		45)	^{93}Nb	4125
9)	^{75}As	3325		46)	^{94}Nb	4128
10)	^{74}Se	3425		47)	^{95}Nb	4131
11)	^{76}Se	3431		48)	^{92}Mo	4225
12)	^{77}Se	3434		49)	^{94}Mo	4231
13)	^{78}Se	3437		50)	^{95}Mo	4234
14)	^{79}Se	3440		51)	^{96}Mo	4237
15)	^{80}Se	3443		52)	^{97}Mo	4240
16)	^{82}Se	3449		53)	^{98}Mo	4243
17)	^{79}Br	3525		54)	^{99}Mo	4246
18)	^{81}Br	3531		55)	^{100}Mo	4249
19)	^{78}Kr	3625		56)	^{99}Tc	4325
20)	^{80}Kr	3631		57)	^{96}Ru	4425
21)	^{82}Kr	3637		58)	^{98}Ru	4431
22)	^{83}Kr	3640		59)	^{99}Ru	4434
23)	^{84}Kr	3643		60)	^{100}Ru	4437
24)	^{85}Kr	3646		61)	^{101}Ru	4440
25)	^{86}Kr	3649		62)	^{102}Ru	4443
26)	^{85}Rb	3725		63)	^{103}Ru	4446
27)	^{86}Rb	3728		64)	^{104}Ru	4449
28)	^{87}Rb	3731		65)	^{105}Ru	4452
29)	^{84}Sr	3825		66)	^{106}Ru	4455
30)	^{86}Sr	3831		67)	^{103}Rh	4525
31)	^{87}Sr	3834		68)	^{105}Rh	4531
32)	^{88}Sr	3837		69)	^{102}Pd	4625
33)	^{89}Sr	3840		70)	^{104}Pd	4631
34)	^{90}Sr	3843		71)	^{105}Pd	4634
35)	^{89}Y	3925		72)	^{106}Pd	4637
36)	^{90}Y	3928		73)	^{107}Pd	4640
37)	^{91}Y	3931		74)	^{108}Pd	4643

Table 3.3: List of fission product materials evaluated by BNL. The list corresponds to the neutron sub-library of the ENDF/B-VII.0 library [1].

No.	Material	MAT		No.	Material	MAT
75)	^{110}Pd	4649		112)	^{123}Te	5234
76)	^{107}Ag	4725		113)	^{124}Te	5237
77)	^{109}Ag	4731		114)	^{125}Te	5240
78)	^{110m}Ag	4735		115)	^{126}Te	5243
79)	^{111}Ag	4737		116)	^{127m}Te	5247
80)	^{106}Cd	4825		117)	^{128}Te	5249
81)	^{108}Cd	4831		118)	^{129m}Te	5253
82)	^{110}Cd	4837		119)	^{130}Te	5255
83)	^{111}Cd	4840		120)	^{132}Te	5261
84)	^{112}Cd	4843		121)	^{127}I	5325
85)	^{113}Cd	4846		122)	^{129}I	5331
86)	^{114}Cd	4849		123)	^{130}I	5334
87)	^{115m}Cd	4853		124)	^{131}I	5337
88)	^{116}Cd	4855		125)	^{135}I	5349
89)	^{113}In	4925		126)	^{123}Xe	5422
90)	^{115}In	4931		127)	^{124}Xe	5425
91)	^{112}Sn	5025		128)	^{126}Xe	5431
92)	^{113}Sn	5028		129)	^{128}Xe	5437
93)	^{114}Sn	5031		130)	^{129}Xe	5440
94)	^{115}Sn	5034		131)	^{130}Xe	5443
95)	^{116}Sn	5037		132)	^{131}Xe	5446
96)	^{117}Sn	5040		133)	^{132}Xe	5449
97)	^{118}Sn	5043		134)	^{133}Xe	5452
98)	^{119}Sn	5046		135)	^{134}Xe	5455
99)	^{120}Sn	5049		136)	^{135}Xe	5458
100)	^{122}Sn	5055		137)	^{136}Xe	5461
101)	^{123}Sn	5058		138)	^{133}Cs	5525
102)	^{124}Sn	5061		139)	^{134}Cs	5528
103)	^{125}Sn	5064		140)	^{135}Cs	5531
104)	^{126}Sn	5067		141)	^{136}Cs	5534
105)	^{121}Sb	5125		142)	^{137}Cs	5537
106)	^{123}Sb	5131		143)	^{130}Ba	5625
107)	^{124}Sb	5134		144)	^{132}Ba	5631
108)	^{125}Sb	5137		145)	^{133}Ba	5634
109)	^{126}Sb	5140		146)	^{134}Ba	5637
110)	^{120}Te	5225		147)	^{135}Ba	5640
111)	^{122}Te	5231		148)	^{136}Ba	5643

Table 3.3: List of fission product materials evaluated by BNL. The list corresponds to the neutron sub-library of the ENDF/B-VII.0 library [1].

No.	Material	MAT		No.	Material	MAT
149)	^{137}Ba	5646		186)	^{153}Sm	6252
150)	^{138}Ba	5649		187)	^{154}Sm	6255
151)	^{140}Ba	5655		188)	^{151}Eu	6325
152)	^{138}La	5725		189)	^{152}Eu	6328
153)	^{139}La	5728		190)	^{153}Eu	6331
154)	^{140}La	5731		191)	^{154}Eu	6334
155)	^{136}Ce	5825		192)	^{155}Eu	6337
156)	^{138}Ce	5831		193)	^{156}Eu	6340
157)	^{139}Ce	5834		194)	^{157}Eu	6343
158)	^{140}Ce	5837		195)	^{152}Gd	6425
159)	^{141}Ce	5840		196)	^{153}Gd	6428
160)	^{142}Ce	5843		197)	^{154}Gd	6431
161)	^{143}Ce	5846		198)	^{155}Gd	6434
162)	^{144}Ce	5849		199)	^{156}Gd	6437
163)	^{141}Pr	5925		200)	^{157}Gd	6440
164)	^{142}Pr	5928		201)	^{158}Gd	6443
165)	^{143}Pr	5931		202)	^{160}Gd	6449
166)	^{142}Nd	6025		203)	^{159}Tb	6525
167)	^{143}Nd	6028		204)	^{160}Tb	6528
168)	^{144}Nd	6031		205)	^{156}Dy	6625
169)	^{145}Nd	6034		206)	^{158}Dy	6631
170)	^{146}Nd	6037		207)	^{160}Dy	6637
171)	^{147}Nd	6040		208)	^{161}Dy	6640
172)	^{148}Nd	6043		209)	^{162}Dy	6643
173)	^{150}Nd	6049		210)	^{163}Dy	6646
174)	^{147}Pm	6149		211)	^{164}Dy	6649
175)	^{148}Pm	6152		212)	^{165}Ho	6725
176)	^{148}Pm	6153		213)	^{166m}Ho	6729
177)	^{149}Pm	6155		214)	^{162}Er	6825
178)	^{151}Pm	6161		215)	^{164}Er	6831
179)	^{144}Sm	6225		216)	^{166}Er	6837
180)	^{147}Sm	6234		217)	^{167}Er	6840
181)	^{148}Sm	6237		218)	^{168}Er	6843
182)	^{149}Sm	6240		219)	^{170}Er	6849
183)	^{150}Sm	6243				

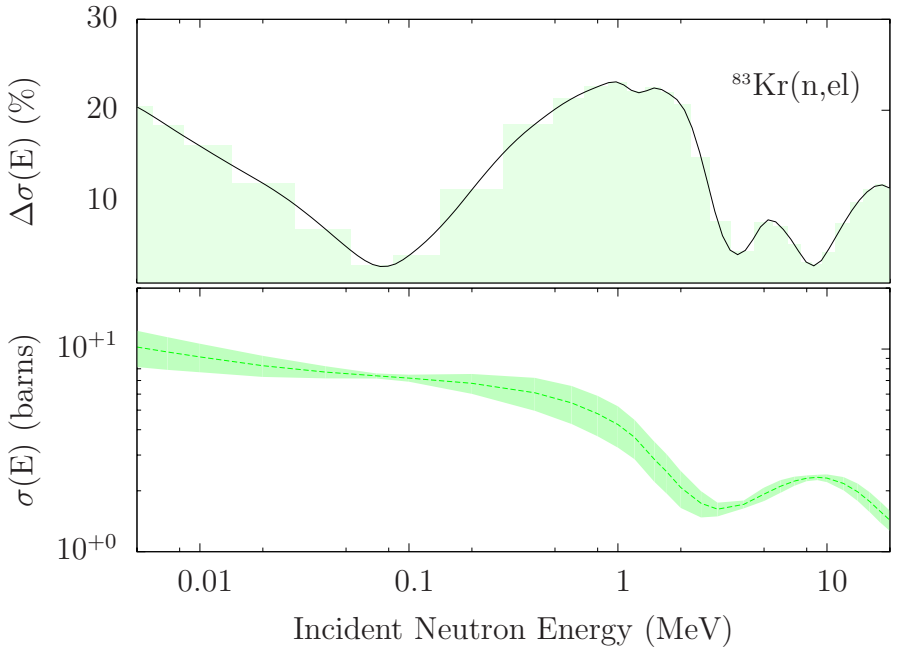

Figure 3.1: Relative uncertainties for ^{83}Kr(n,el) and ^{83}Kr(n,inl) obtained with the EMPIRE-KALMAN method.

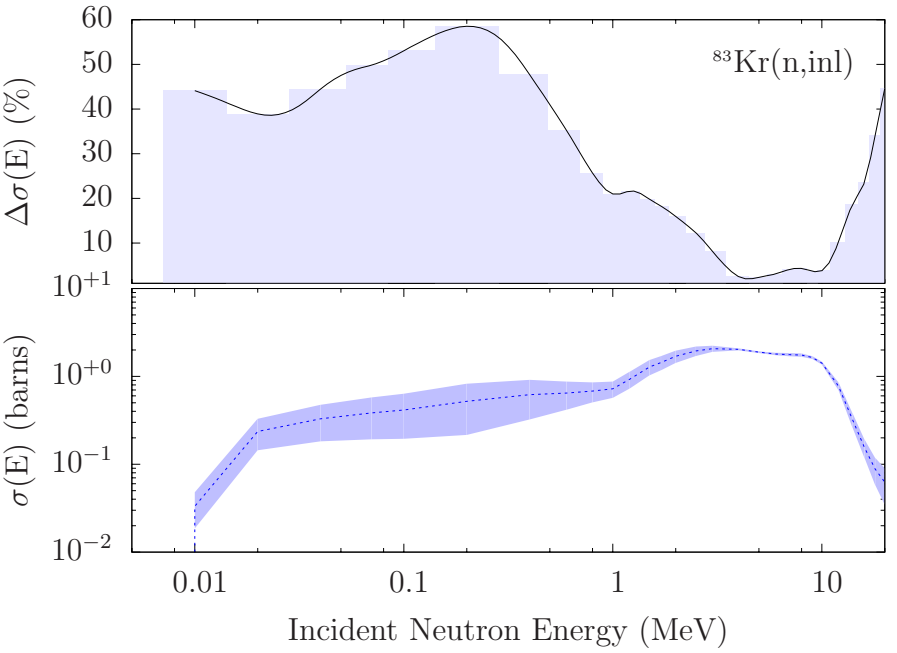

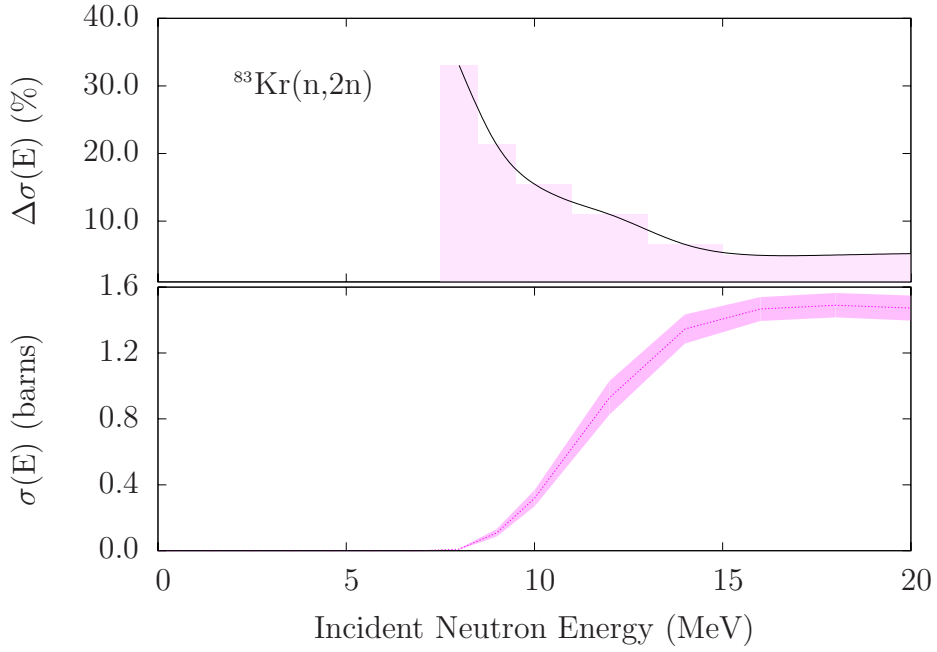

Figure 3.2: Relative uncertainties for ^{83}Kr(n,2n) and ^{83}Kr(n,γ) obtained with the EMPIRE-KALMAN method.

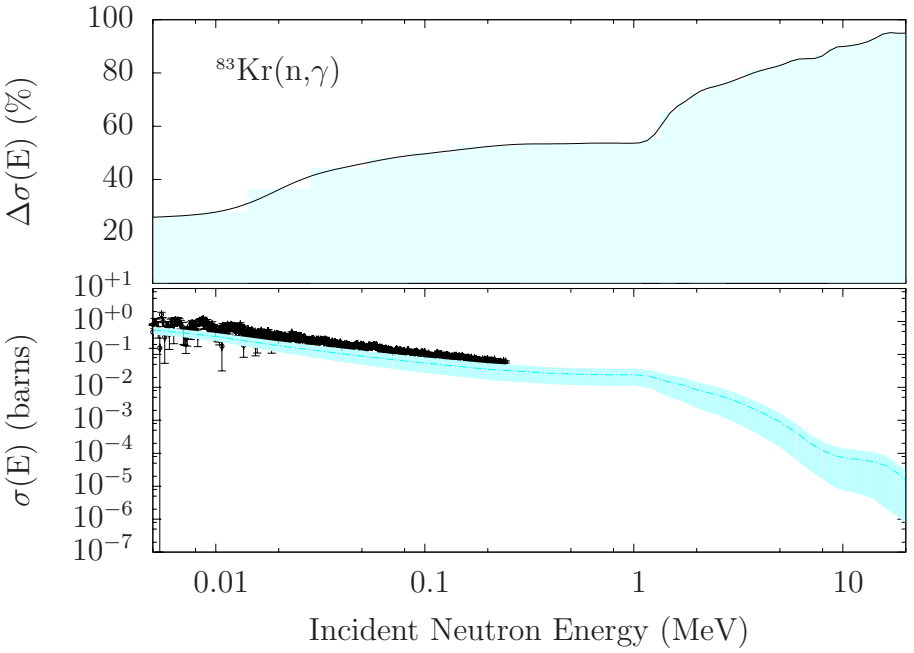

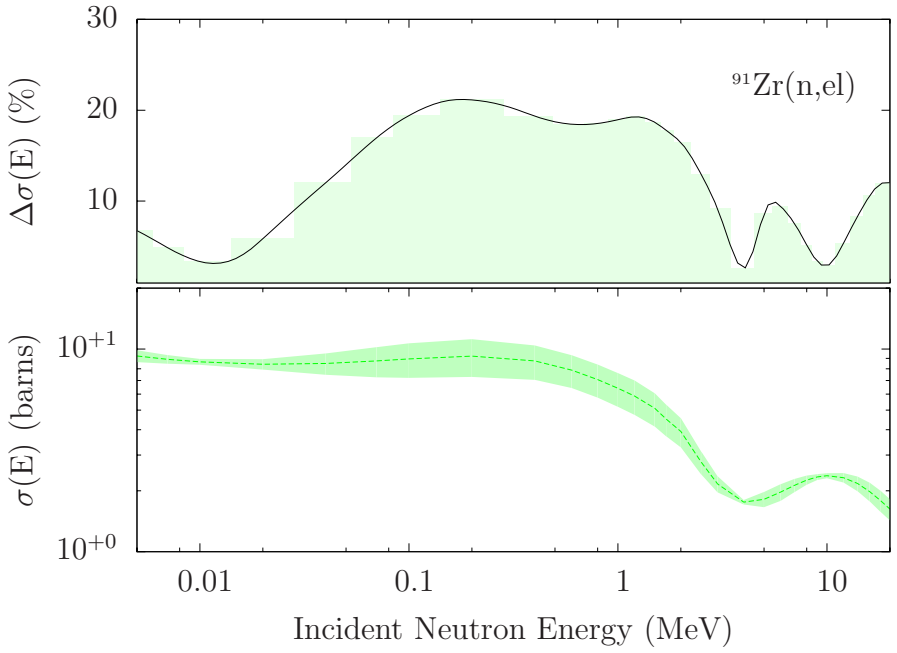

Figure 3.3: Relative uncertainties for ^{91}Zr(n,el) and ^{91}Zr(n,inl) obtained with the EMPIRE-KALMAN method.

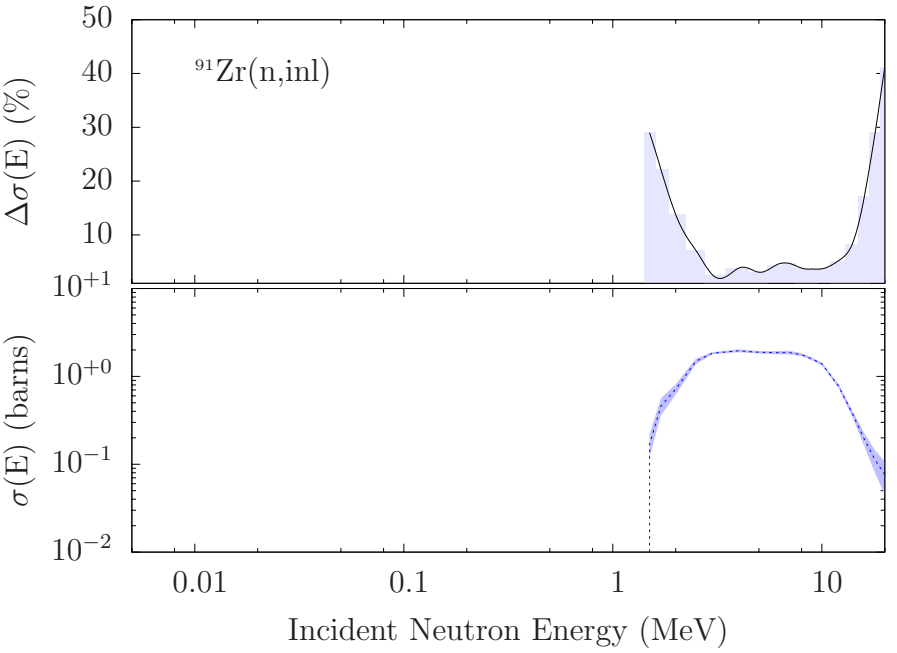

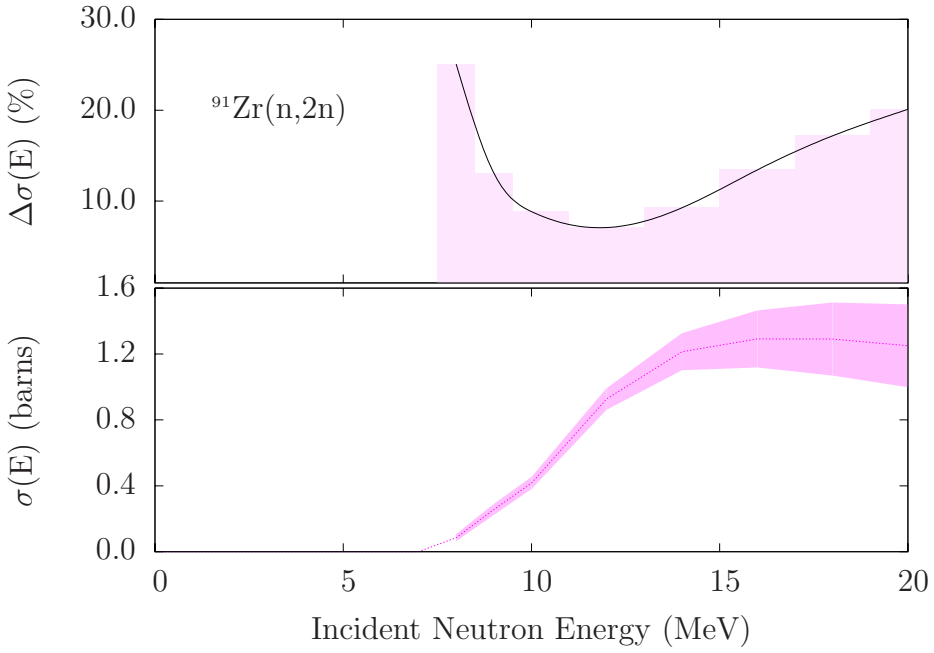

Figure 3.4: Relative uncertainties for ^{91}Zr(n,2n) and ^{91}Zr(n,γ) obtained with the EMPIRE-KALMAN method.

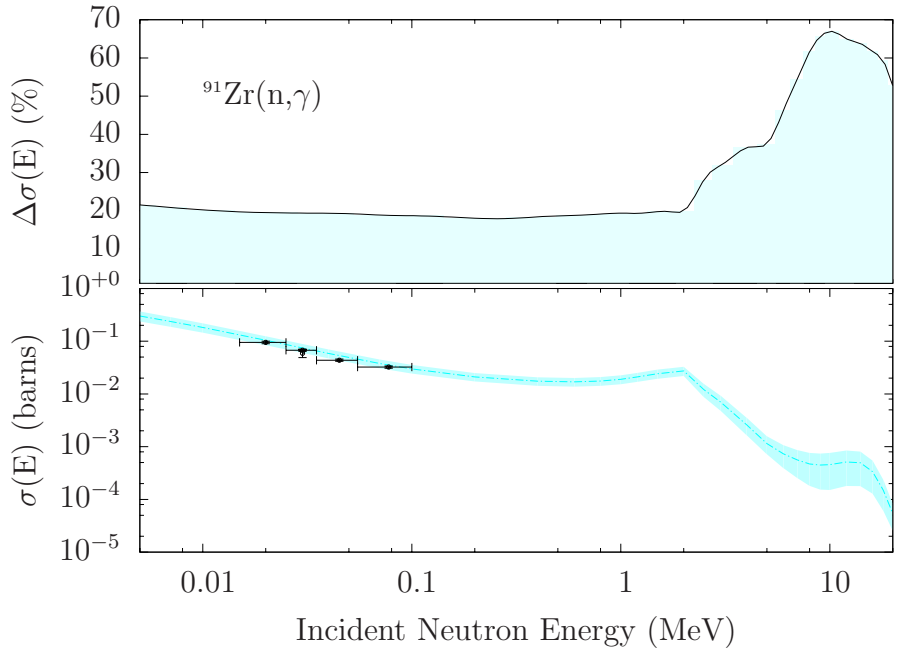

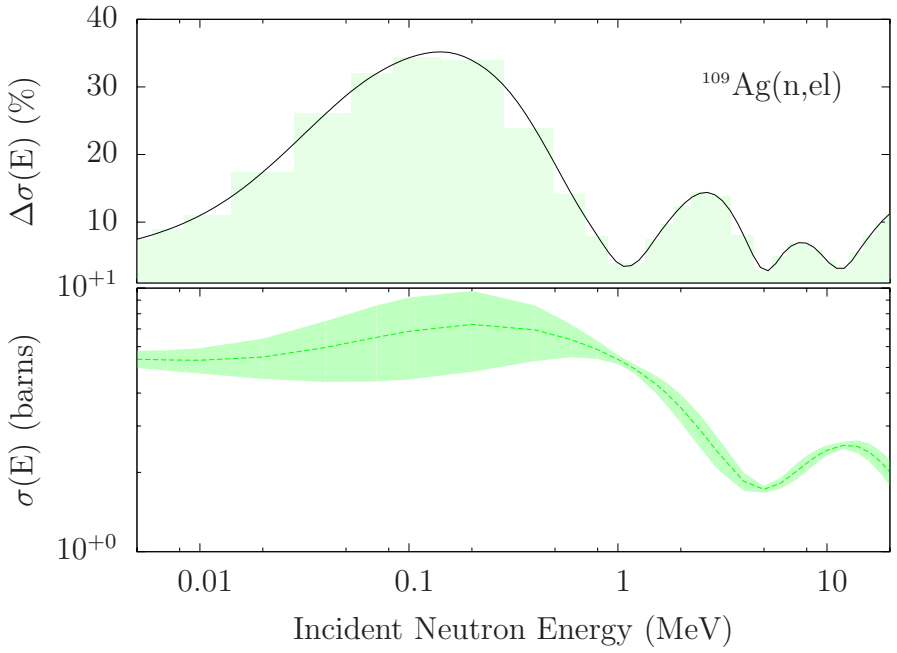

Figure 3.5: Relative uncertainties for ^{109}Ag(n,el) and ^{109}Ag(n,inl) obtained with the EMPIRE-KALMAN method.

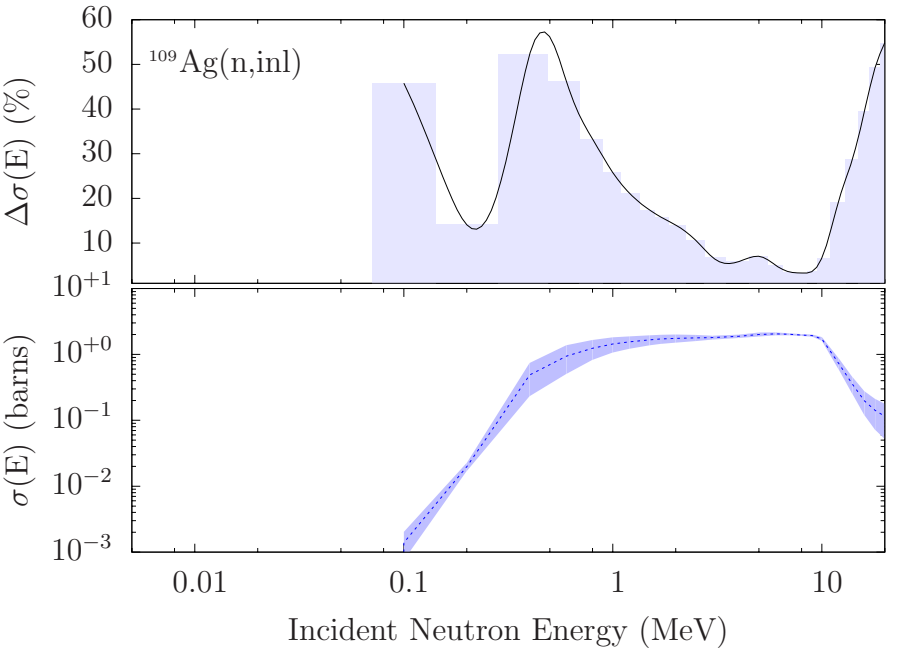

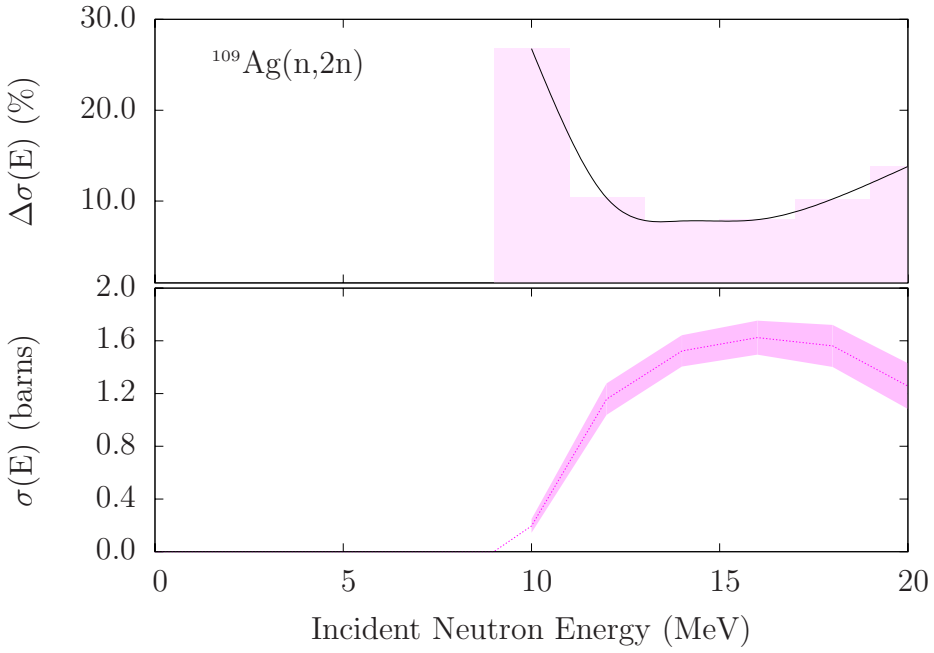

Figure 3.6: Relative uncertainties for ^{109}Ag(n,2n) and ^{109}Ag(n,γ) obtained with the EMPIRE-KALMAN method.

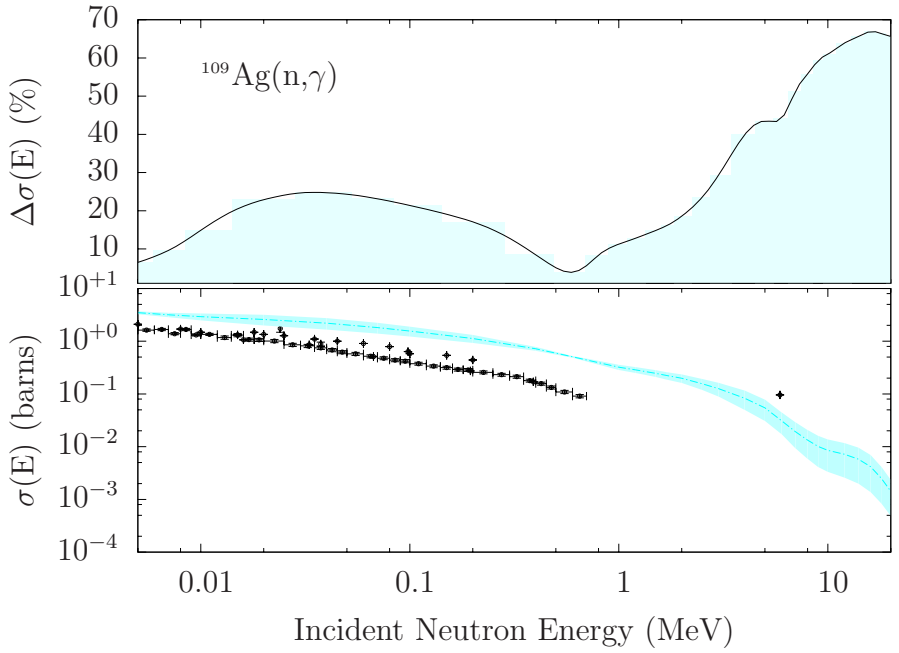

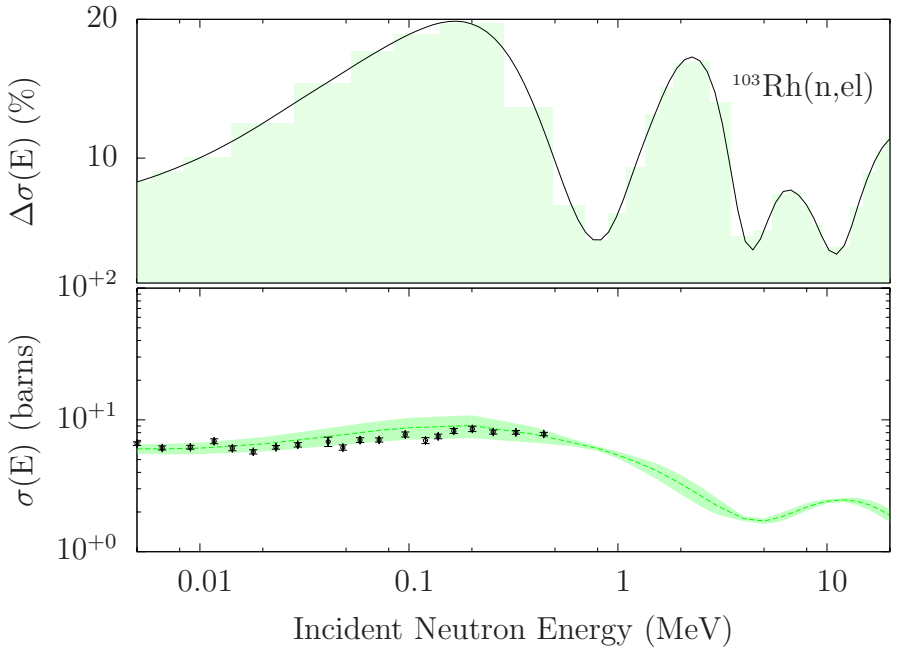

Figure 3.7: Relative uncertainties for ^{103}Rh(n,el) and ^{103}Rh(n,inl) obtained with the EMPIRE-KALMAN method.

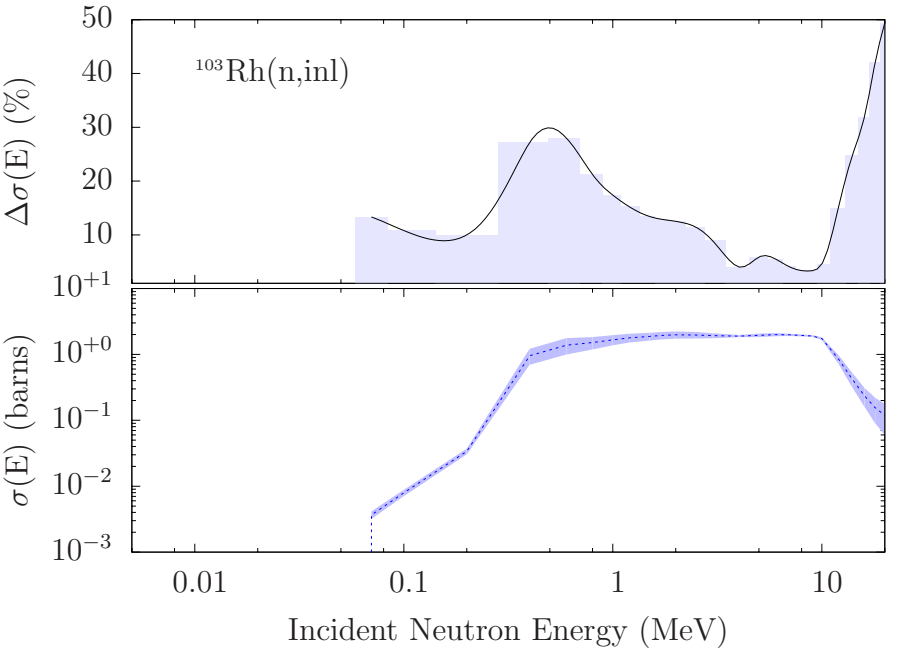

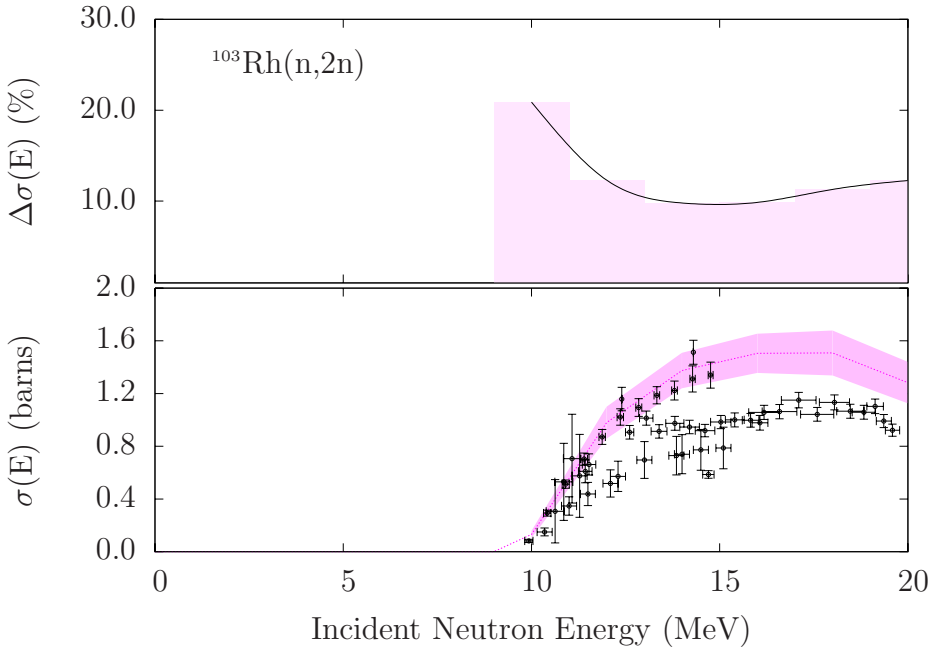

Figure 3.8: Relative uncertainties for ^{103}Rh(n,2n) and ^{103}Rh(n,γ) obtained with the EMPIRE-KALMAN method.

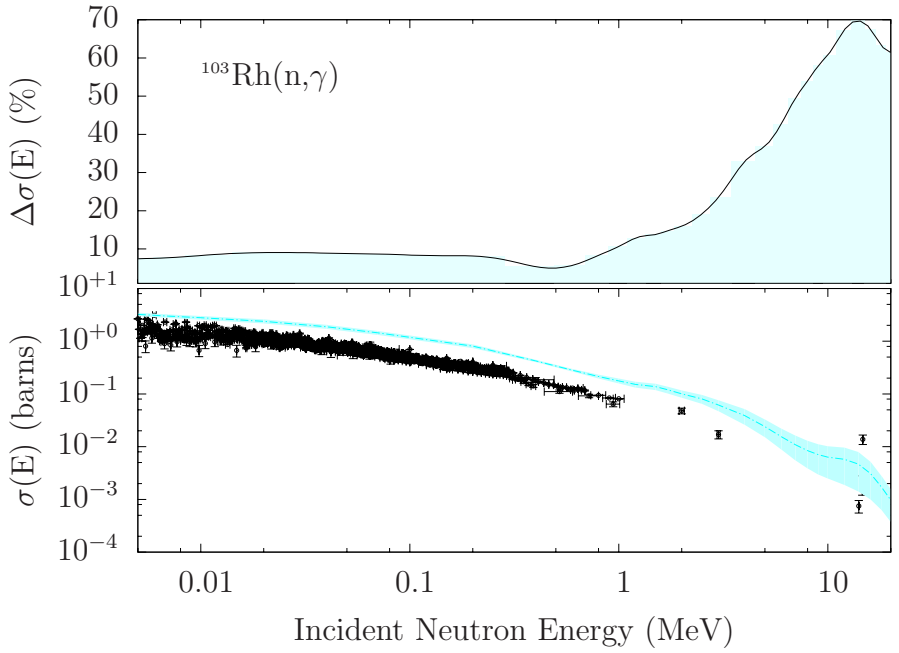

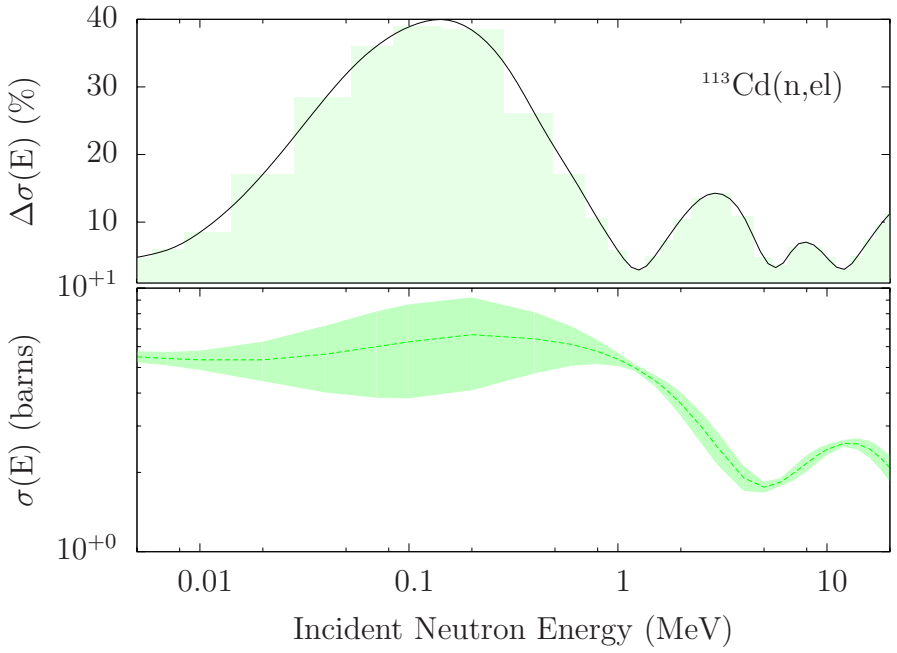

Figure 3.9: Relative uncertainties for ^{113}Cd(n,el) and ^{113}Cd(n,inl) obtained with the EMPIRE-KALMAN method.

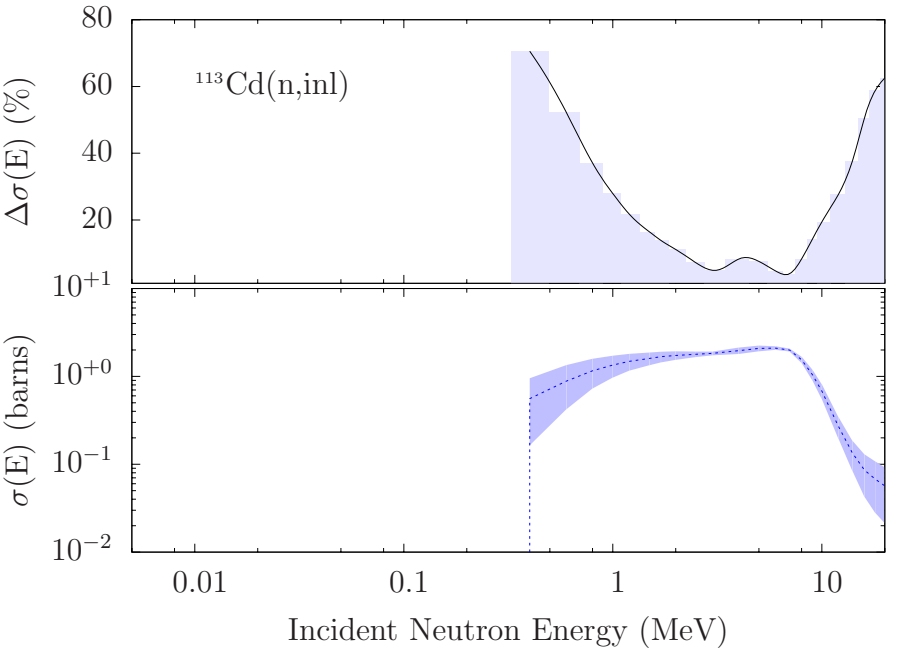

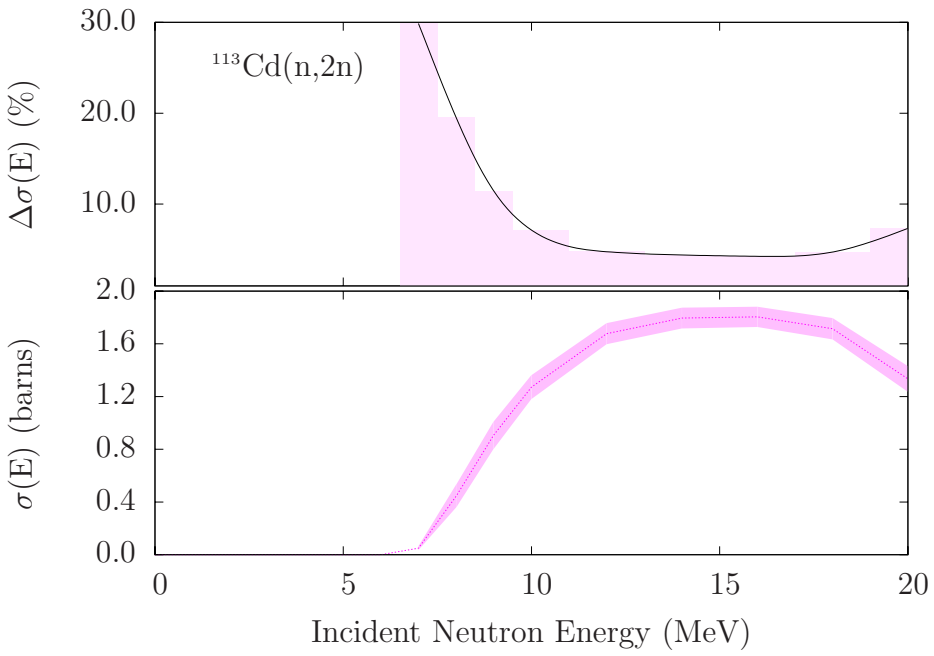

Figure 3.10: Relative uncertainties for ^{113}Cd(n,2n) and ^{113}Cd(n,γ) obtained with the EMPIRE-KALMAN method.

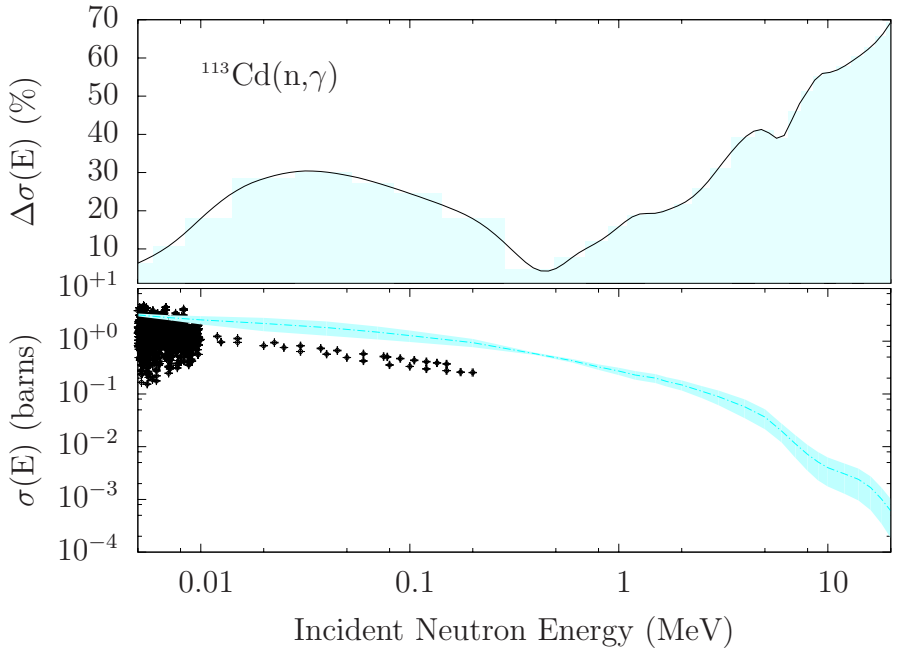

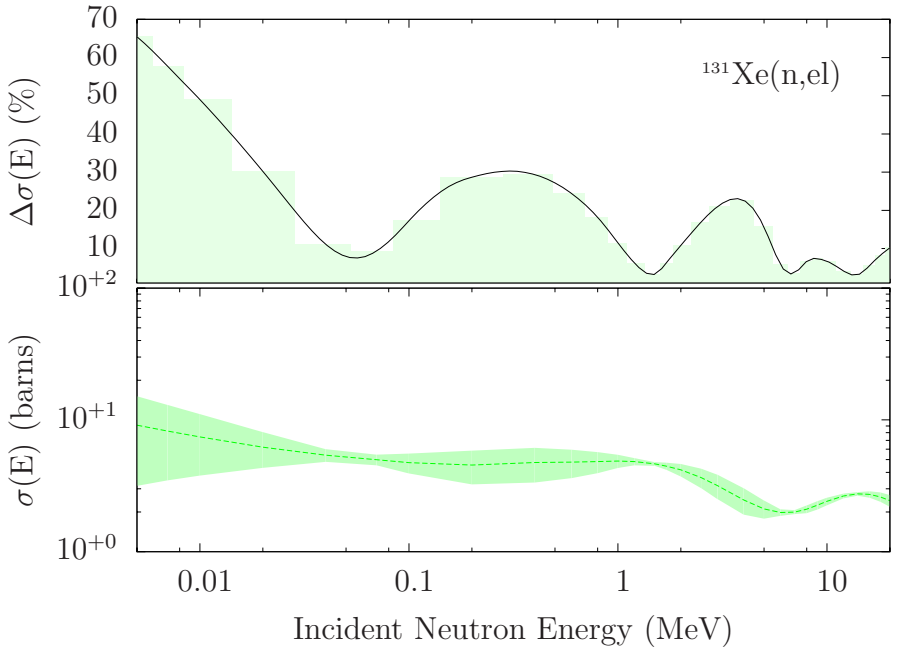

Figure 3.11: Relative uncertainties for ^{131}Xe(n,el) and ^{131}Xe(n,inl) obtained with the EMPIRE-KALMAN method.

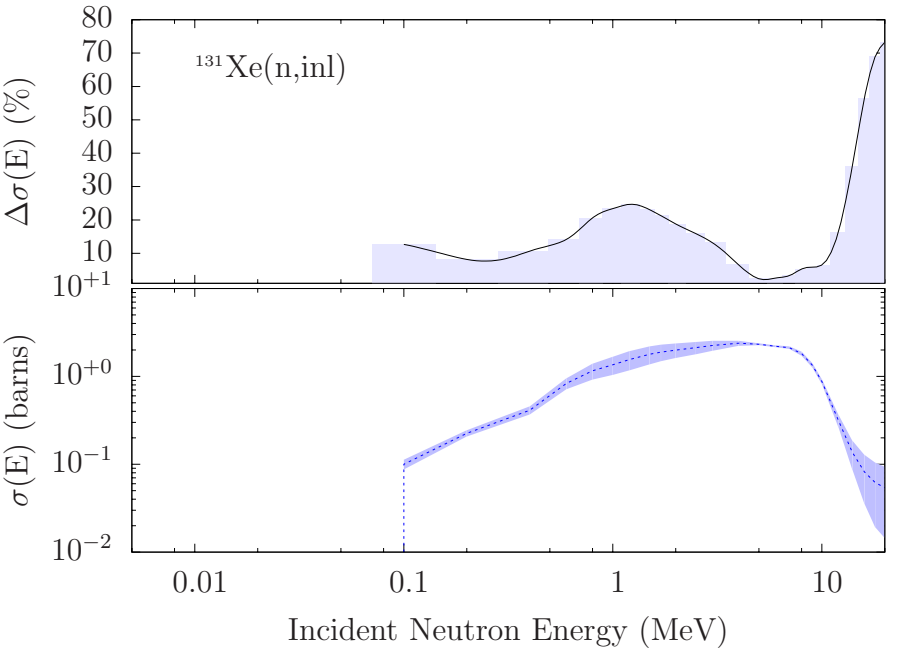

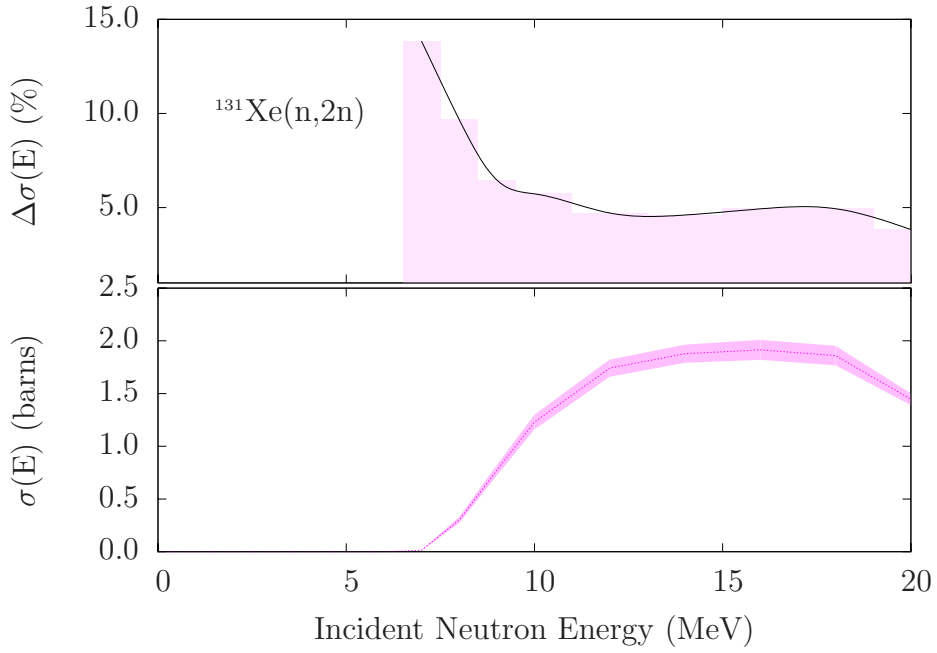

Figure 3.12: Relative uncertainties for ^{131}Xe(n,2n) and ^{131}Xe(n,γ) obtained with the EMPIRE-KALMAN method.

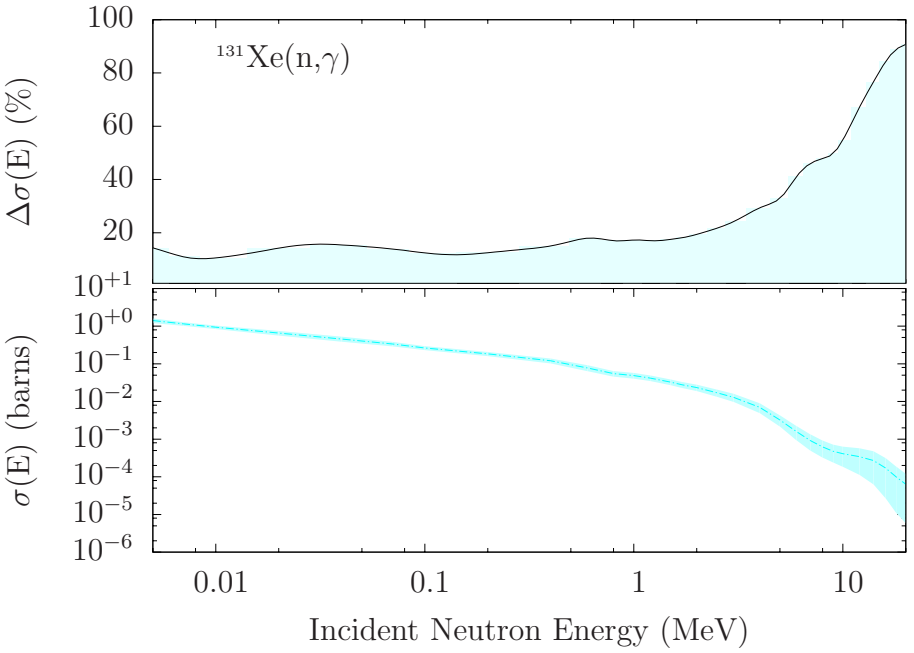

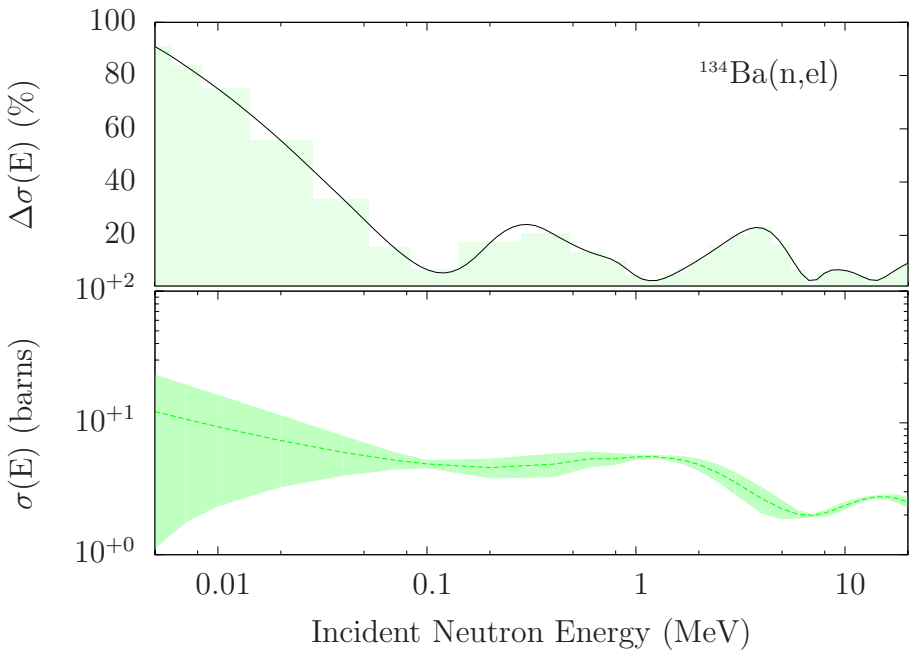

Figure 3.13: Relative uncertainties for ^{134}Ba(n,el) and ^{134}Ba(n,inl) obtained with the EMPIRE-KALMAN method.

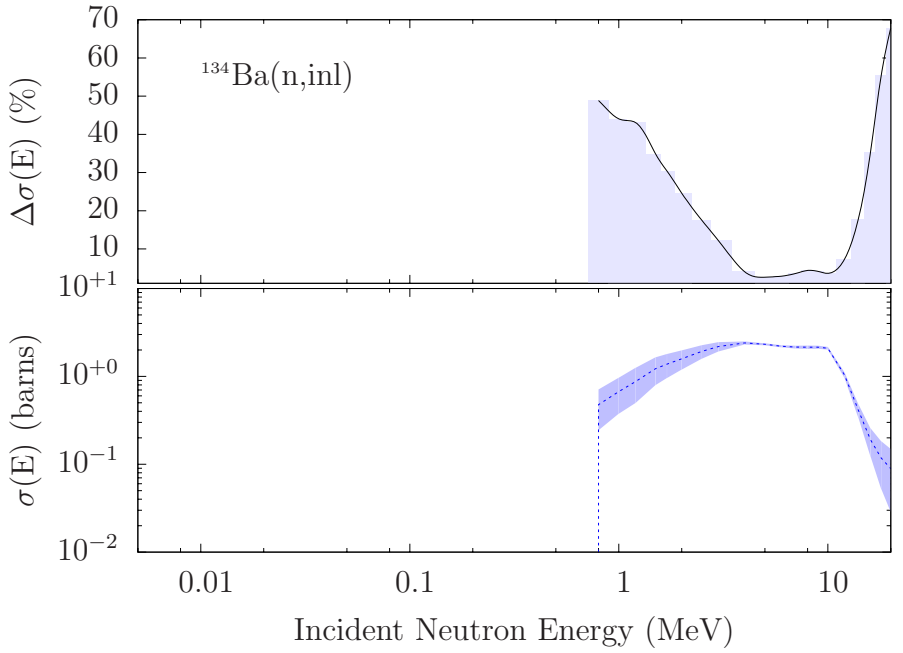

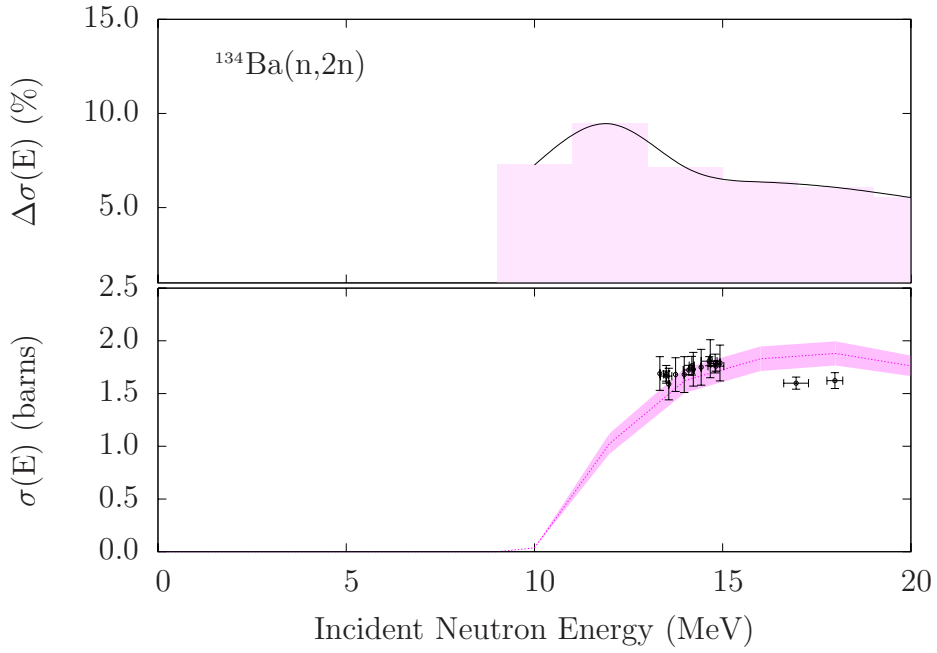

Figure 3.14: Relative uncertainties for ^{134}Ba(n,2n) and ^{134}Ba(n,γ) obtained with the EMPIRE-KALMAN method.

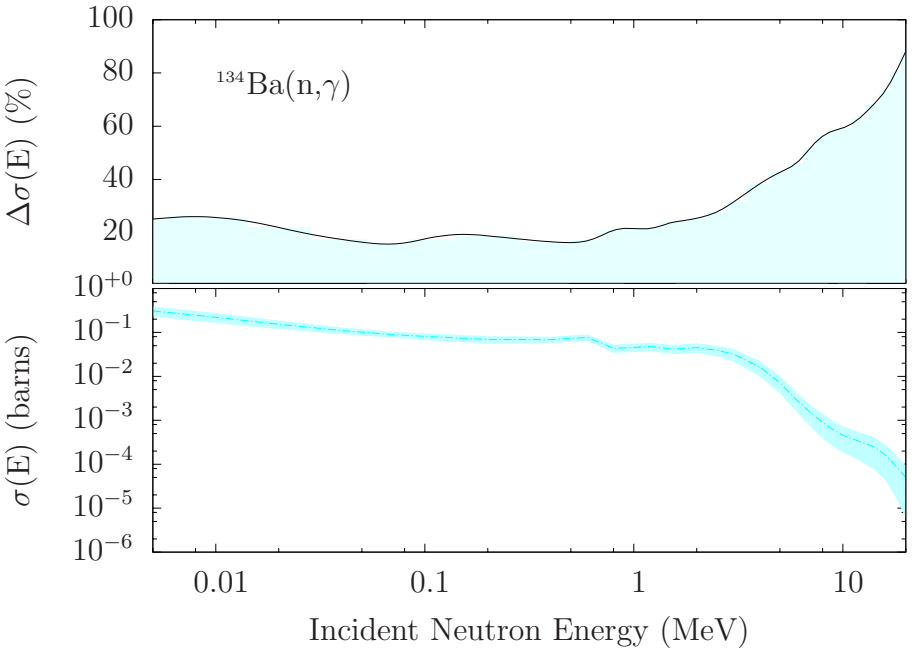

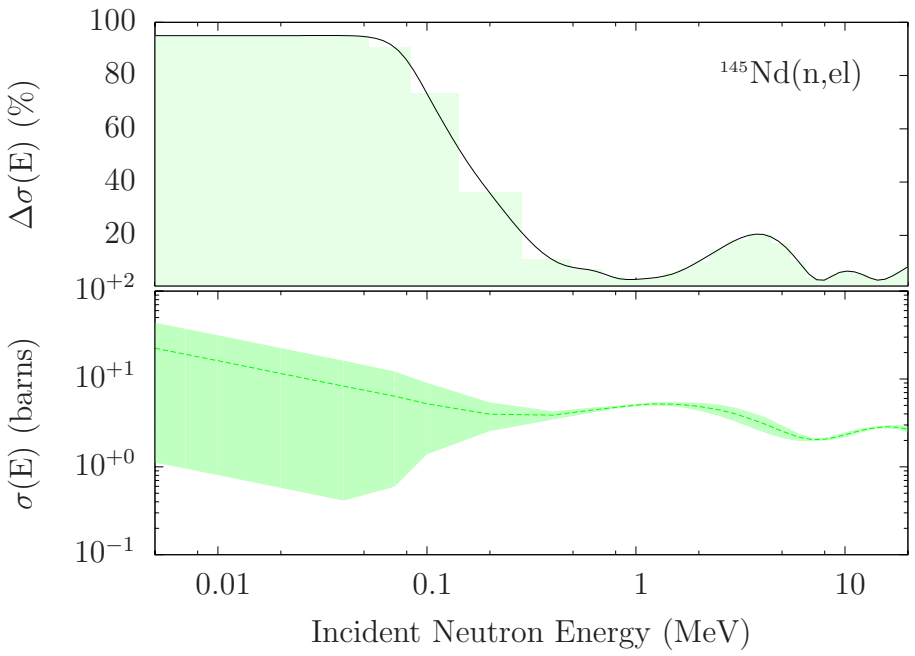

Figure 3.15: Relative uncertainties for ^{145}Nd(n,el) and ^{145}Nd(n,inl) obtained with the EMPIRE-KALMAN method.

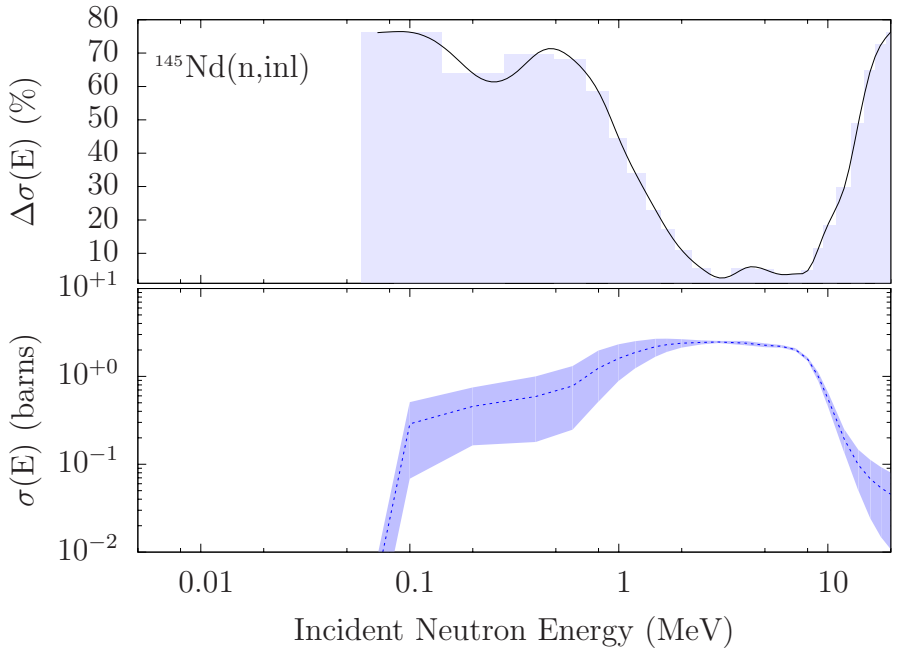

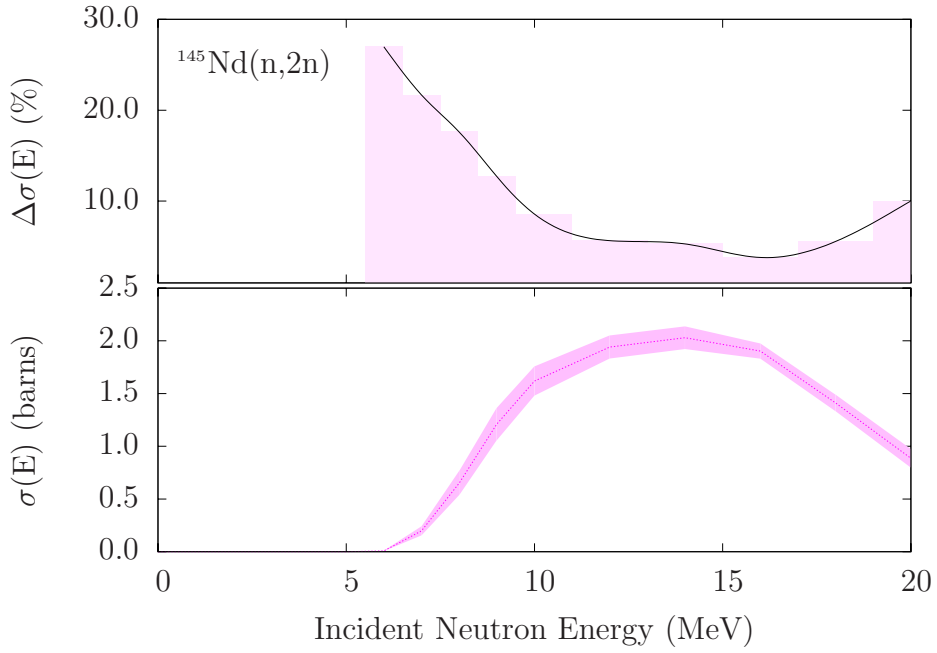

Figure 3.16: Relative uncertainties for ^{145}Nd(n,2n) and ^{145}Nd(n,γ) obtained with the EMPIRE-KALMAN method.

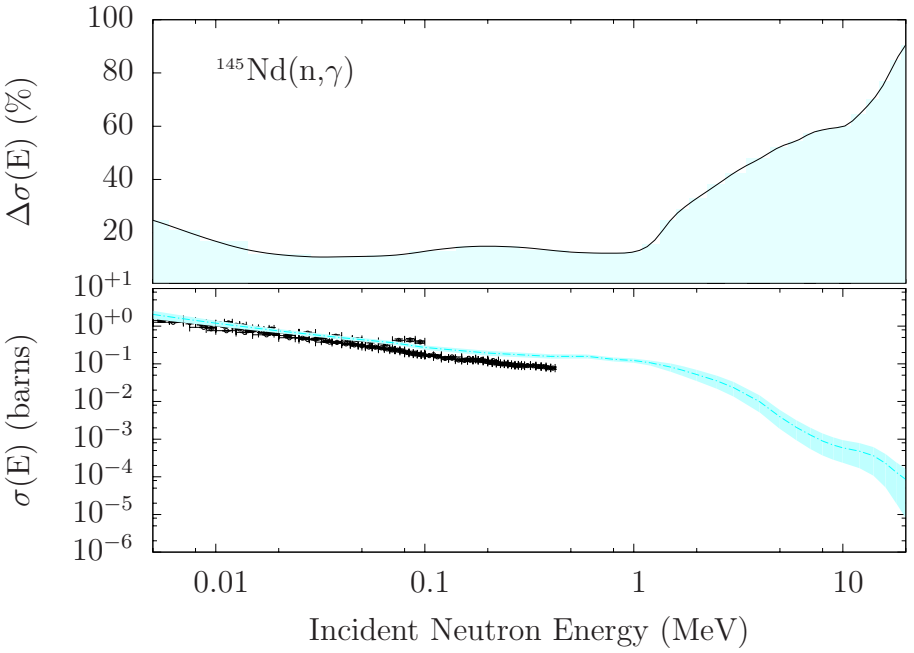

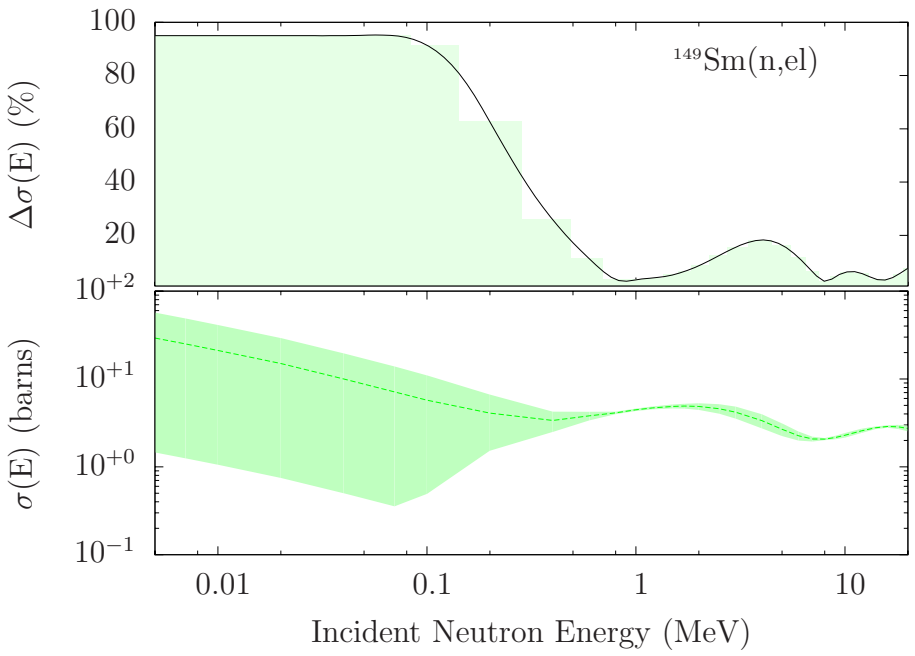

Figure 3.17: Relative uncertainties for ^{149}Sm(n,el) and ^{149}Sm(n,inl) obtained with the EMPIRE-KALMAN method.

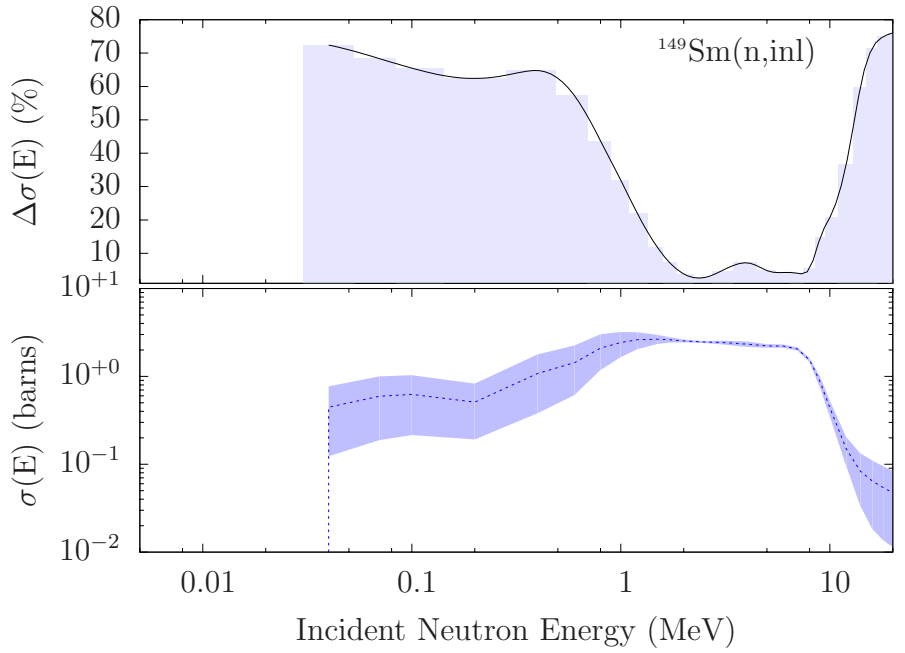

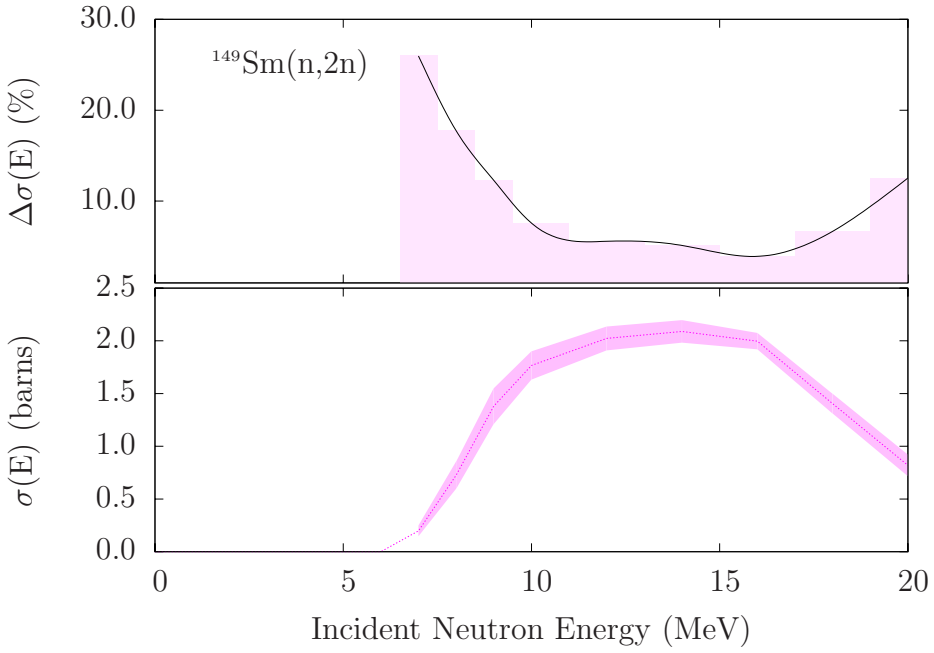

Figure 3.18: Relative uncertainties for ^{149}Sm(n,2n) and ^{149}Sm(n,γ) obtained with the EMPIRE-KALMAN method.

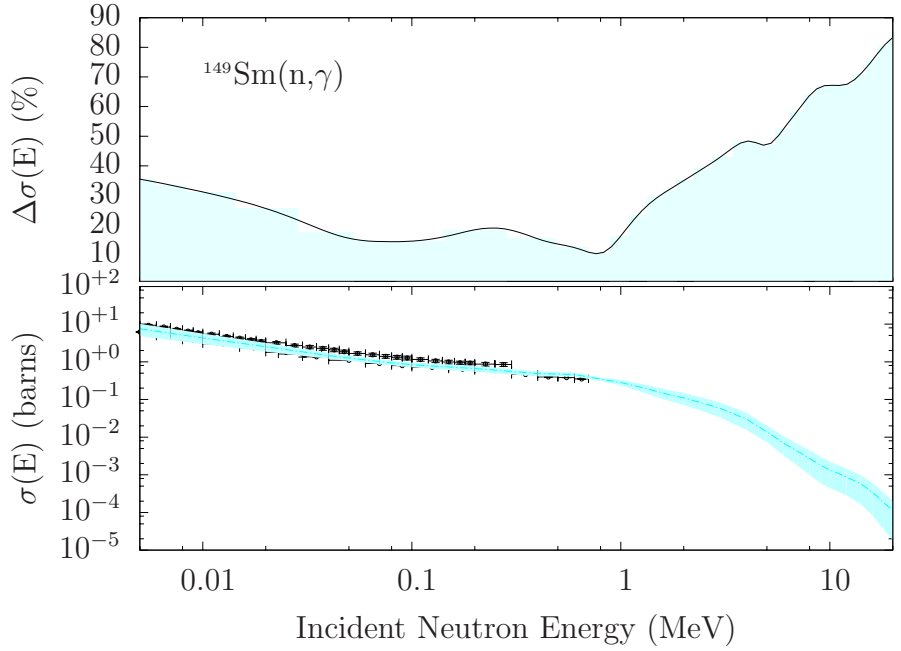

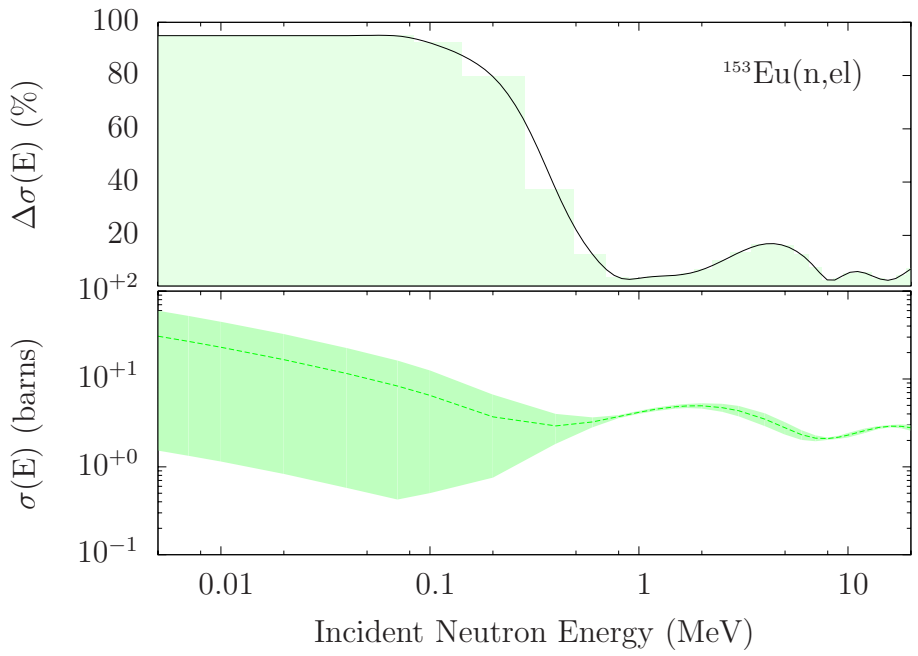

Figure 3.19: Relative uncertainties for ^{153}Eu(n,el) and ^{153}Eu(n,inl) obtained with the EMPIRE-KALMAN method.

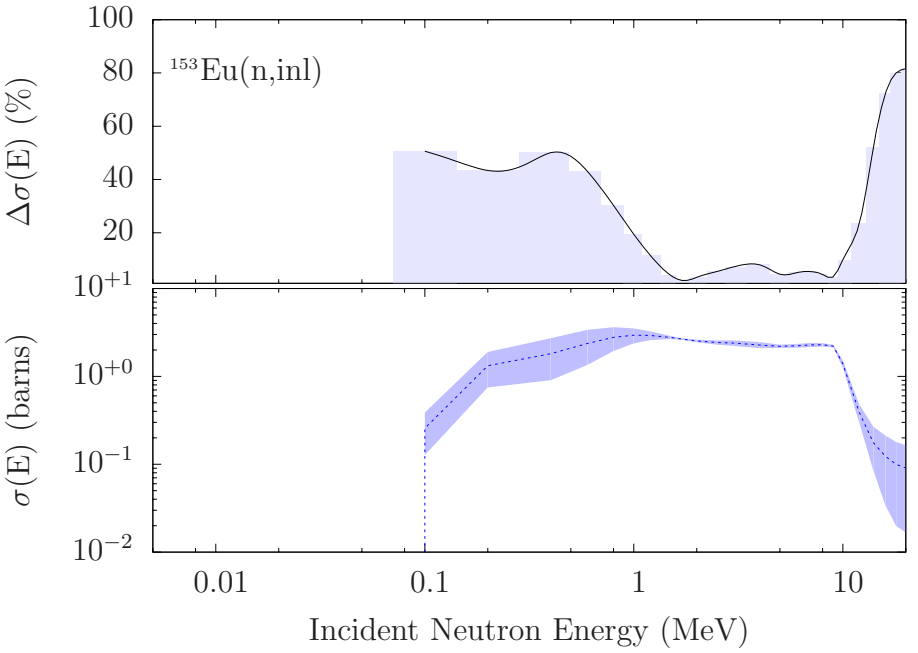

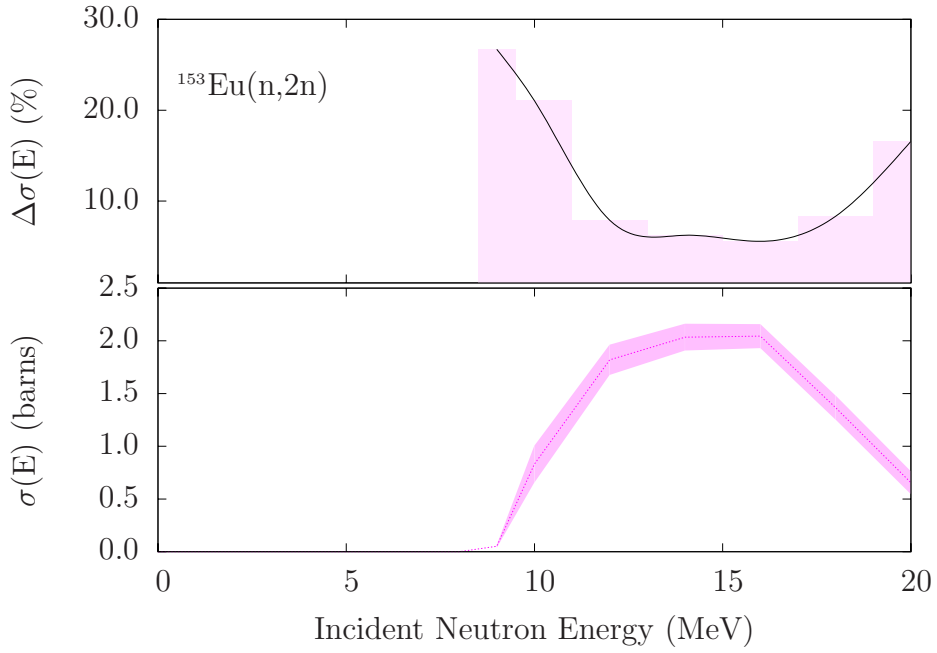

Figure 3.20: Relative uncertainties for ^{153}Eu(n,2n) and ^{153}Eu(n,γ) obtained with the EMPIRE-KALMAN method.

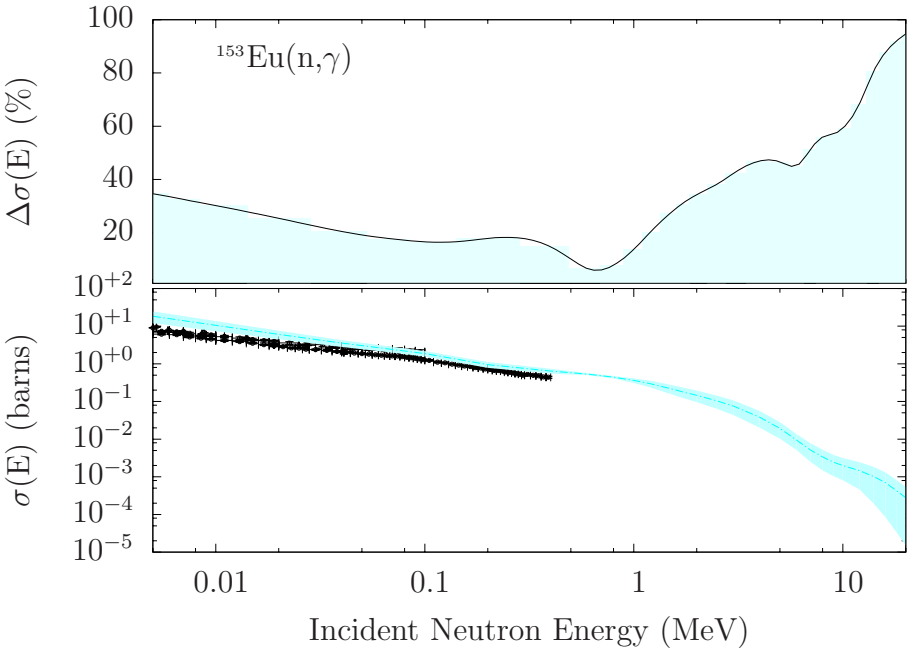

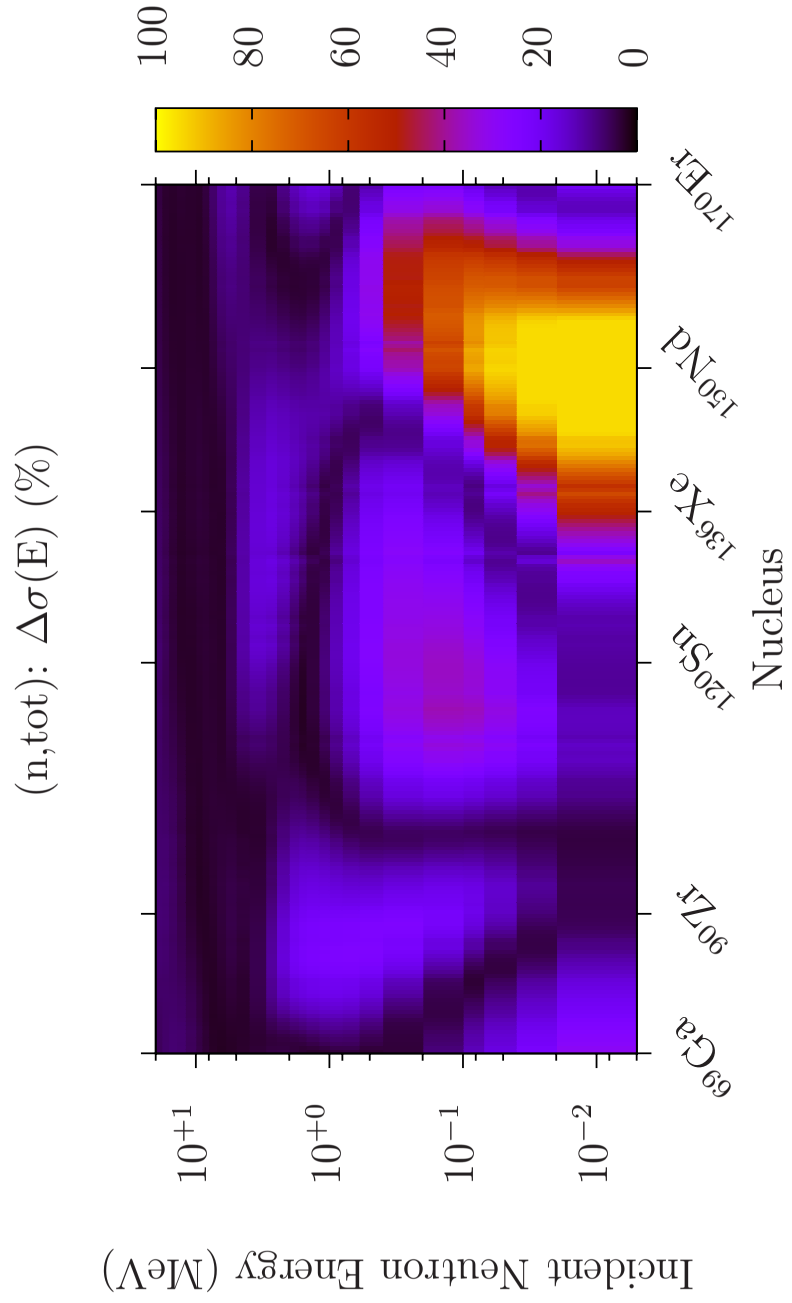

Figure 3.21: Relative uncertainties for the total cross sections on 219 fission product materials obtained with the EMPIRE-KALMAN method in the fast neutron energy region.

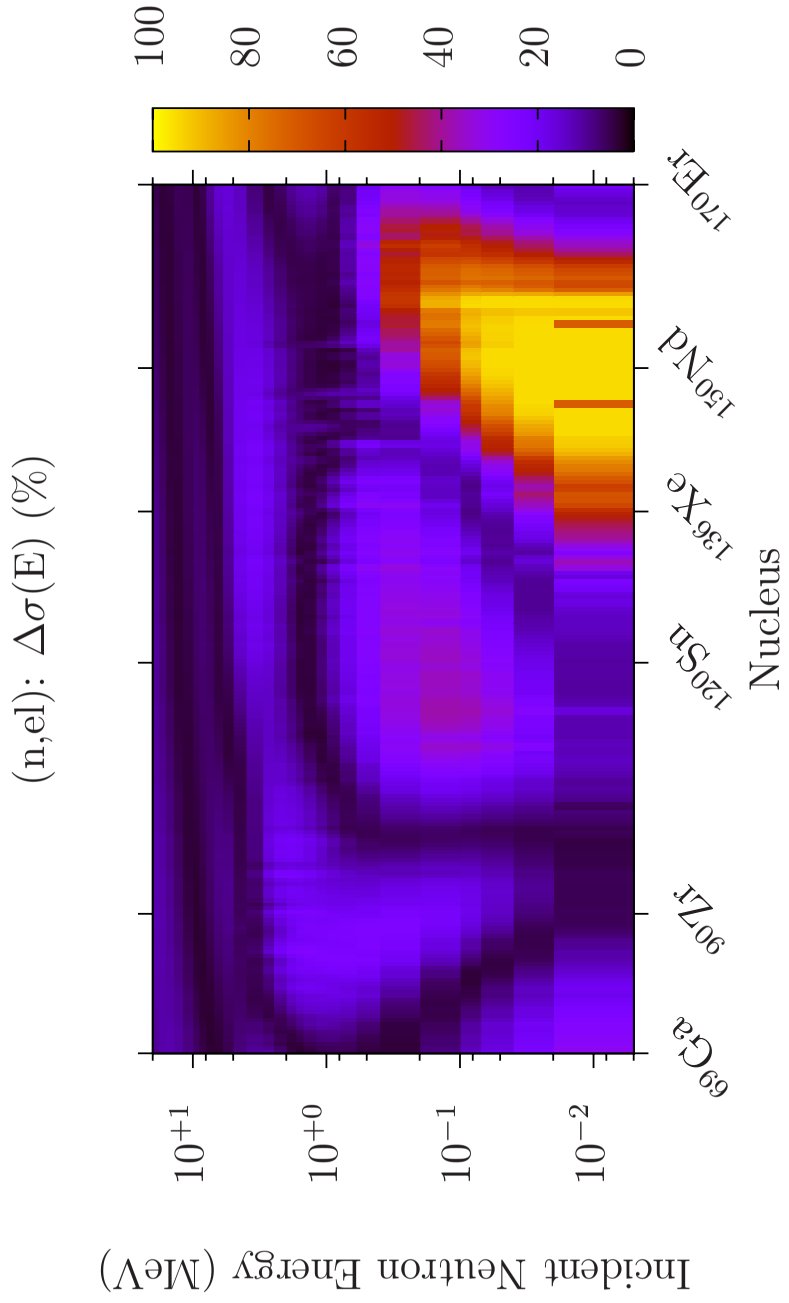

Figure 3.22: Relative uncertainties for the elastic cross sections on 219 fission product materials obtained with the EMPIRE-KALMAN method in the fast neutron energy region.

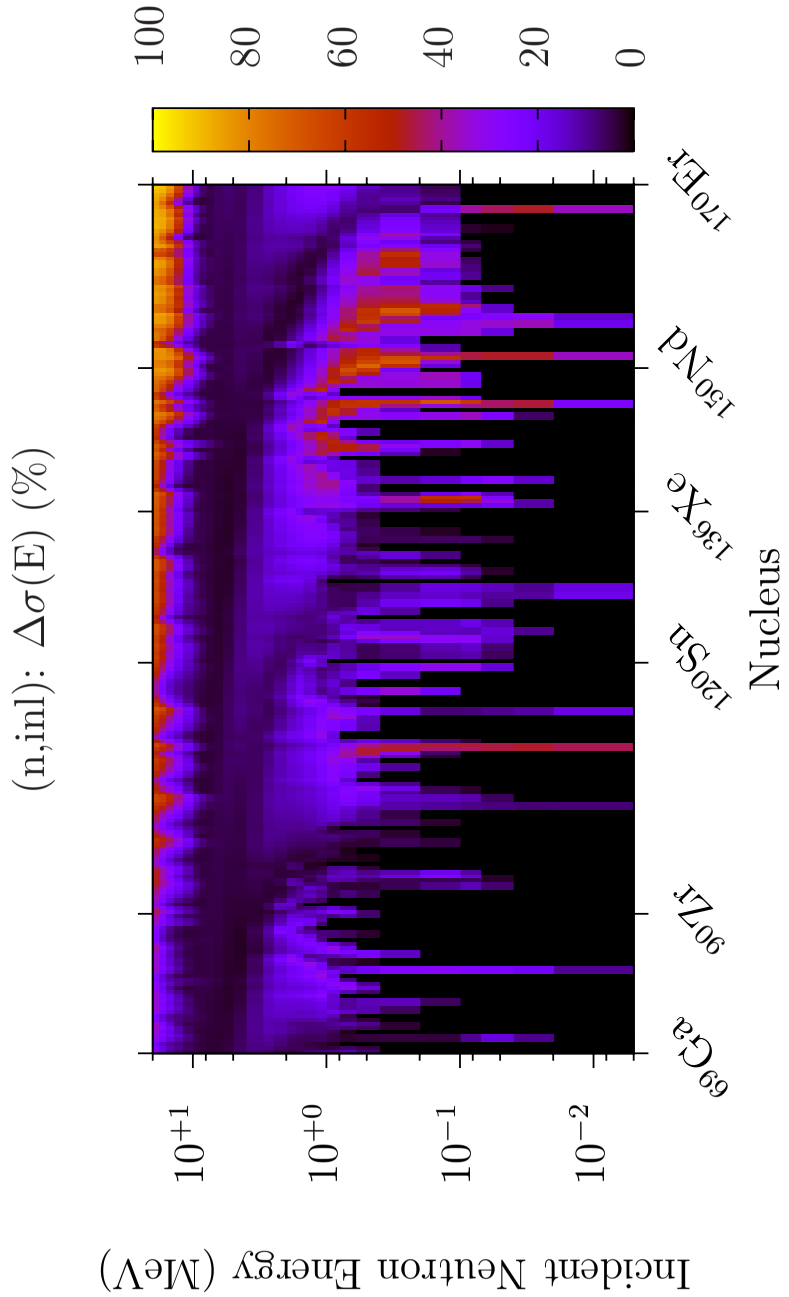

Figure 3.23: Relative uncertainties for the inelastic cross sections on 219 fission product materials obtained with the EMPIRE- KALMAN method in the fast neutron energy region.

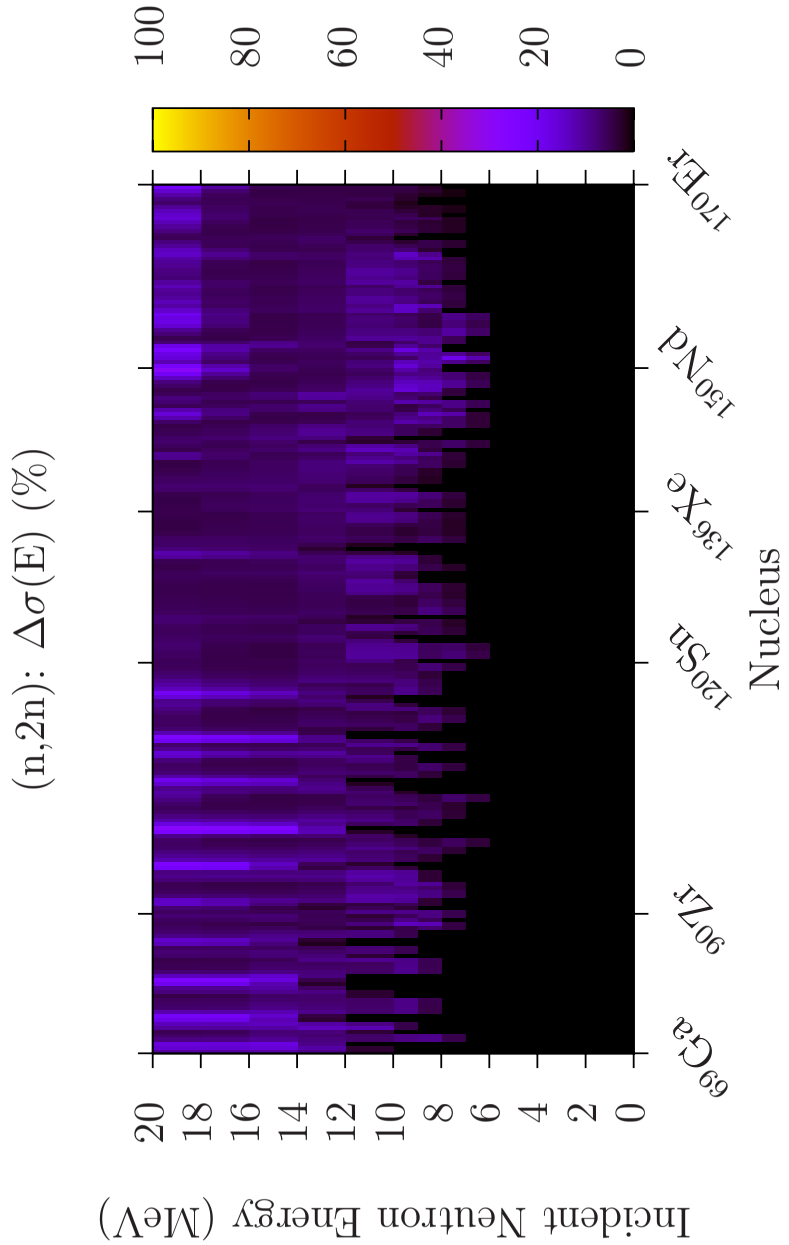

Figure 3.24: Relative uncertainties for the (n,2n) cross sections on 219 fission product materials obtained with the EMPIRE-KALMAN method in the fast neutron energy region.

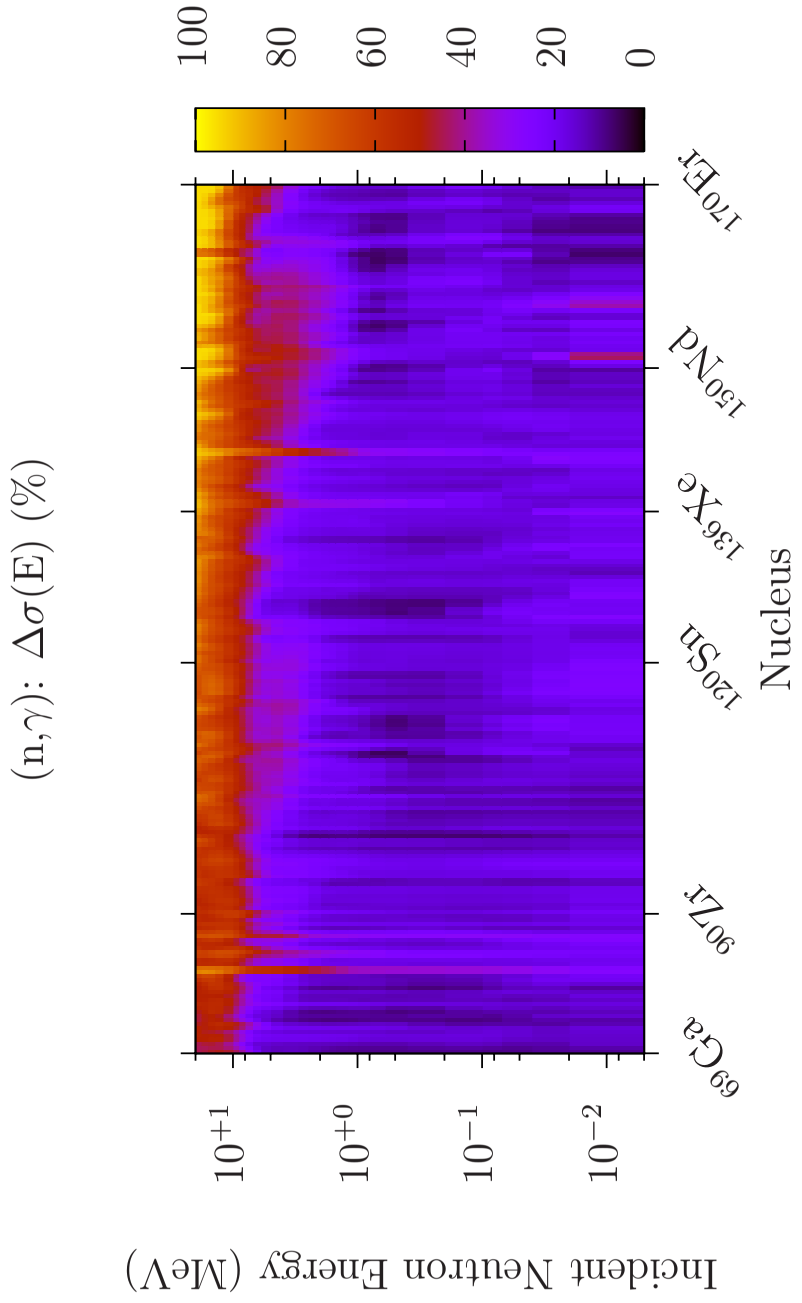

Figure 3.25: Relative uncertainties for the capture cross sections on 219 fission product materials obtained with EMPIRE-KALMAN method in the fast neutron energy region.

Chapter 4

Conclusions and outlook

We have applied the EMPIRE-KALMAN method to produce simple, yet consistent set of fast neutron covariance matrices for 219 fission products including the ENDF/B-VII.0 library. To the best of our knowledge this is the first covariance effort on such a scale. Our results are based on model calculations and depend on the assumed uncertainties of the model parameters.

The experimental data were used only globally to ensure that calculated cross section uncertainties are, on average, in reasonable agreement with the spread of measurements and their uncertainties. Since the same global set of model parameters and related uncertainties was used for all 219 nuclides the calculated cross section uncertainties deviate from the estimated uncertainties derived from the experimental results. This is a natural price to be paid for the global approach.

Our results reveal intriguing structure in the uncertainties plotted against incident energy and mass number (the atomic number dependence might also be possible). In particular, we note very similar patterns observed in the total and elastic channels. A reflection of these patterns is also found in the inelastic one. The (n,2n) and capture channels do not seem to be affected by the structure seen in the total and elastic channels but instead they display short range fluctuations in function of mass number - high and low uncertainties alternate producing vertical lines on the plots. Since all nuclei were treated on the same footing using the same set of models and default set of parameters, it should be possible to explain the patterns in terms of physics underlying our calculations. For example, the structure showing up in the total and elastic channels arises from the optical model and we understand the origin of deep minima in the cross section uncertainties at certain energies.

Mass dependence of the energies at which these minima occur is most likely responsible for creation of the characteristic patterns in Figs. 3.21 and 3.22.

In future, we intend to produce neutron cross section covariance estimates for the remaining 57 structural and 28 heavy materials. In this way we would complete our obligation to the low fidelity project (304 materials). In addition, we would like to address the intriguing structure observed in cross section uncertainties and find out its physics background.

List of Figures

List of Tables

Acknowledgments

The authors would like to thank R. Little and T. Kawano (LANL), M. Dunn and M. Williams (ORNL) as well as R. McKnight (ANL) for stimulating discussions and collaboration in this project.

This work was supported by the DOE-NNSA within the Nuclear Criticality Safety Program and this support is gratefully acknowledged. The National Nuclear Data Center is sponsored by the Office of Nuclear Physics, Office of Science of the U.S. Department of Energy under contract No. DE-AC02-98CH10886 with Brookhaven Science Associates, LLC.

Bibliography

[1] M.B Chadwick, P. Obložinský, and M. Herman et al. ENDF/B-VII: Next Generation Evaluated Nuclear Data Library for Nuclear Science and Technology. *Nuclear Data Sheets*, **107**(12):2931–3060, December 2006.

[2] M. Herman, R. Capote, and B.V. Carlson et al. EMPIRE: Nuclear Reaction Model Code System for Data Evaluation (to be published). *Nuclear Data Sheets*, 2007.

[3] T. Kawano and K. Shibata. Covariance Evaluation System [in Japanese]. *JAERI-Data/Code 97-037*, September 1997.

[4] A.J. Koning and J.P. Delaroche. Local and global nucleon optical model from 1 keV to 200 MeV. *Nucl. Phys. A*, **713**:231–310, January 2003.

[5] M.T. Pigni, M. Herman, P. Obložinský, and D. Rochman. Extensive set of low-fidelity covariances in fast neutron region. In *8th International Meeting on Nuclear Applications of Accelarator Technology, Pocatello, ID 2007*. July 2007.